Biochimica et Biophysica Acta 1847 (2015) 262–275

Contents lists available at ScienceDirect

Biochimica et Biophysica Acta

journal homepage: www.elsevier.com/locate/bbabio

Carotenoid triplet states in photosystem II: Coupling with low-energy states of the core complex

Stefano Santabarbara [a,*], Alessandro Agostini [b], Anna Paola Casazza [c], Giuseppe Zucchelli [a], Donatella Carbonera [b,**]

[a] Istituto di Biofisica, Consiglio Nazionale delle Ricerche, Via Celoria 26, 20133 Milan, Italy
[b] Department of Chemical Sciences, Università di Padova, Via Marzolo 1, 35131 Padova, Italy
[c] Istituto di Biologia e Biotecnologia Agraria, Consiglio Nazionale delle Ricerche, Via Bassini 15a, 20133 Milano, Italy

ARTICLE INFO

Article history:
Received 25 September 2014
Received in revised form 19 November 2014
Accepted 21 November 2014
Available online 3 December 2014

Keywords:
Photosystem II
Photosystem II core complex
Carotenoid
Triplet state
Triplet state quenching
Optically Detected Magnetic Resonance

ABSTRACT

The photo-excited triplet states of carotenoids, sensitised by triplet–triplet energy transfer from the chlorophyll triplet states, have been investigated in the isolated Photosystem II (PSII) core complex and PSII–LHCII (Light Harvesting Complex II) supercomplex by Optically Detected Magnetic Resonance techniques, using both fluorescence (FDMR) and absorption (ADMR) detection. The absence of Photosystem I allows us to reach the full assignment of the carotenoid triplet states populated in PSII under steady state illumination at low temperature. Five carotenoid triplet (^{3}Car) populations were identified in PSII–LHCII, and four in the PSII core complex. Thus, four ^{3}Car populations are attributed to β-carotene molecules bound to the core complex. All of them show associated fluorescence emission maxima which are relatively red-shifted with respect to the bulk emission of both the PSII–LHCII and the isolated core complexes. In particular the two populations characterised by Zero Field Splitting parameters $|D| = 0.0370–0.0373\ cm^{-1}/|E| = 0.00373–0.00375\ cm^{-1}$ and $|D| = 0.0381–0.0385\ cm^{-1}/|E| = 0.00393–0.00389\ cm^{-1}$, are coupled by singlet energy transfer with chlorophylls which have a red-shifted emission peaking at 705 nm. This observation supports previous suggestions that pointed towards the presence of long-wavelength chlorophyll spectral forms in the PSII core complex. The fifth ^{3}Car component is observed only in the PSII–LHCII supercomplex and is then assigned to the peripheral light harvesting system.

1. Introduction

Photosystem II (PSII) is a macromolecular light-dependent oxido-reductase which catalyses the oxidation of water to molecular oxygen and protons, and the reduction of plastoquinone to plastoquinol e.g. [1–3]. From a structural point of view PSII can be seen as composed of two moieties: i) the *core* that serves both as photo-catalytic centre and proximal light harvesting antenna to the reaction centre (RC), and appears to be substantially conserved throughout evolution e.g. [4,5], and ii) an external antenna, whose function is only that of light harvesting, and which varies greatly amongst species as an adaptation to the spectral quality of incident radiation in different ecological environments e.g. [6,7].

The core complex is composed of over 20 subunits [1–5], binds about 40 chlorophyll (Chl) *a* and 10 β-carotene (β-Car) molecules, together with the other cofactors required for electron transfer, including two pheophytin and two plastoquinone molecules, a cytochrome (Cyt b_{559}), a Fe atom and a 4Mn–1Ca cluster, which is the site of water splitting e.g. [8,9]. Four subunits bind the vast majority of the pigments: the CP43 and CP47 complexes that compose the proximal antenna and the D1D2Cytb_{559} complex, which harbours all of the electron transfer cofactors [1–5,8,9].

In the green lineage, the external antenna is composed of Chl *a*/*b*-binding complexes [3,11–14], which are the product of the nuclear gene family known as *lhcb* [6,7]. The PSII external antenna contains several components. The principal component, called Light Harvesting Complex II (LHCII), is a trimer and is bound with a stoichiometry of 2–4 trimers per core complex [3,15,16]. Each monomeric unit binds 8 Chl *a*, and 6 Chl *b* as well as four oxygenated carotenoids (xanthophylls), two lutein, one neoxanthin and one violaxanthin molecules [3,11–14]. The latter can be exchanged with zeaxanthin depending on the growth conditions [17–19]. The other PSII antenna complexes, CP24, CP26 and CP29, are all isolated as monomers and bind with 1:1 stoichiometry to

Abbreviations: PSII(I), Photosystem II(I); LHC, Light Harvesting Complex; RC, reaction centre; Chl, chlorophyll; Car, carotenoid; Xan, xanthophyll; ODMR, Optically Detected Magnetic Resonance; FDMR/ADMR, Fluorescence/Absorption Detected Magnetic Resonance; ZFS, Zero Field Splitting; MIF, microwave-induced fluorescence spectrum; T − S, Triplet minus Singlet; NPQ, Non-Photochemical Quenching; TTET, triplet–triplet energy transfer

* Corresponding author. Tel.: +39 0250314857; fax: +39 0250314812.
** Corresponding author. Tel.: +39 498275144; fax: +39 498275161.
E-mail addresses: stefano.santabarbara@cnr.it (S. Santabarbara), donatella.carbonera@unipd.it (D. Carbonera).

http://dx.doi.org/10.1016/j.bbabio.2014.11.008
0005-2728/

the core complex [3,15,16]. Like LHCII, albeit with a different stoichiometric ratio, the monomeric antennae bind, on average, 10–14 pigments per protein, both Chl *a* and Chl *b*, with ratios going from 1.2 to 2.2 and xanthophylls with ratios of 2–3 molecules per complex [3,11–14].

The carotenoids that are bound both to the core and to the external antenna of higher plants play several roles in the photosynthetic apparatus, particularly in PSII. They are involved in light harvesting of the portion of the incident solar spectrum in the blue-green region [19,20]. However, the spectral overlap with the so-called Soret band of Chl *a* and Chl *b* is significant and the increase in the antenna bandwidth is therefore limited overall [21]. Xanthophylls (Xan) are also involved in processes that regulate the efficiency of light harvesting in response to the increase in intensity of the incident radiation, such as Non-Photochemical Quenching (NPQ) (reviewed in Refs. [17–19]). One clear evidence is the enzymatic conversion of violaxanthin to zeaxanthin when the system is exposed to high irradiance regimes, concomitantly with the acidification of the thylakoid lumen [17–19,22]. Moreover, xanthophylls, either lutein or zeaxanthin, have been proposed to play a direct role in NPQ, representing the effective quenching site either through a singlet–singlet (Xan–Chl) energy transfer mechanism e.g. [23–25], or being partner in the formation of a Chl–Xan charge–transfer complex e.g. [26,27]. It has been also suggested that the carotenoid conformation (cis–trans isomerisation, bond twisting) can affect the chromophores binding within the LHC complexes and hence the chromophore–chromophore interactions, leading to the formation of singlet excited state quenchers (reviewed in Ref. [23]). Their involvement in controlling the fine "packing" of the antenna, mediating different interactions between adjacent complexes, has also been discussed [28]. Therefore, independently from the mechanism, which is much debated, the involvement of carotenoids in the NPQ process is generally accepted.

Carotenoids also have an important structural role, stabilising the folding of pigment binding proteins e.g. [29–33]. This has been demonstrated both in vitro by reconstitution experiments of LHC complexes [29,30], as well as in vivo in mutants affected in the carotenoid biosynthesis [31–33].

Certainly, a central role of carotenoids in the photosynthetic apparatus is the quenching of the Chl triplet state (^{3}Chl) through the triplet–triplet energy transfer (TTET) mechanism (reviewed in Refs. [20,34,35]). The direct population of the carotenoid triplet state (^{3}Car) by intersystem crossing (ISC) is a low probability event, due to the very short lifetime of the excited state of these molecules, that is dominated by internal conversion [20,34,35]. Energy transfer from the ^{3}Chl, which is populated with a yield of ~0.6 in the absence of other quenching mechanisms [36,37], is efficient in photosynthetic systems [38–40] because of the short average inter-pigment distances and because the ^{3}Car lays at an energy level which is below that of ^{3}Chl. It is established that the ^{3}Chl is an efficient sensitiser of singlet oxygen ($^1O_2$), which is an highly reactive species and one of the principal actors in photo-oxidative stress [41,42]. On the other hand, the energy level of the ^{3}Car present in photosynthetic complexes is too low to interact with molecular oxygen. Therefore, the quenching of the ^{3}Chl state by TTET to the ^{3}Car is of fundamental importance under physiological perspective. Indeed, the population of ^{3}Car under illumination is well documented both in relatively intact preparations, such as thylakoid membranes e.g. [38–40,43,44], as well as in isolated pigment–protein complexes where it has been investigated intensively e.g. [45–57].

However, the determination of specific Chl–Car interactions and the identification of the molecules involved in TTET are usually cumbersome due to the severe spectral "congestion" determined by the overlap in the absorption spectrum of different Chl forms, as well as different carotenoids, bound to oxygenic photosystems. Such difficulties can be in part overcome by the use of time-resolved magnetic resonance techniques, since the signal arising from the ^{3}Car is strongly polarized and the polarisation is extremely sensitive to the orientation of donor and acceptor molecules in the pair [58]. This allows the identification of the chromophores involved in the energy transfer process, provided that a structural model of the complex is known which sufficient accuracy. The approach has been successfully applied to the study of isolated LHCII and other antenna complexes e.g. [59–62].

An alternative approach is that of using techniques that allow the correlation of parameters characterising the electron spin of the chromophore with the optical properties of either the chromophore itself (i.e. ^{3}Car) or the sensitiser molecule (^{3}Chl). One such technique is Optically Detected Magnetic Resonance (ODMR), which is extremely selective for the detection of photo-excited triplet states (reviewed in Refs. [63–65]; a description of the basic principles of the ODMR technique is presented in Supporting information, Appendix 1). ODMR allows precise estimation of the zero-field splitting (ZFS) parameters that determine the energy split between the triplet sublevels and depend on the unpaired spin distribution with respect to the chromophore molecular frame. In recent years, the use of this technique has allowed the investigation of both ^{3}Car and ^{3}Chl in intact systems, such as the thylakoid membranes [65–69]. Using this spectroscopic method, particularly by fluorescence detection (FDMR), it was possible to identify the ^{3}Chl states populated in both Photosystem I (PSI) and PSII under ambient redox conditions [66–68]. These ^{3}Chl states were suggested to be involved in photo-oxidative stress [70]. It was also possible to detect a ^{3}Chl associated with the reaction centre of PSII under non-reducing conditions [66,67,71]. This ^{3}Chl shows a remarkably fast relaxation [66,67,71] with respect to the ^{3}Chl observed under reducing conditions typically employed to induce charge recombination e.g. [67,72–74].

Although the fluorescence yield of carotenoids is extremely low and therefore almost undetectable, especially in crowded chromophore–protein complexes, it is still possible to monitor ^{3}Car by FDMR, detecting the fluorescence emission of Chl molecules [45–48,65]. This is because the change in the mean rate of the ^{3}Car decay, induced by resonance conditions, affects the steady-state population of the singlet excited states of the Chl fluorescent molecules to which Cars are coupled by energy transfer (Fig. 1). Employing the FDMR technique it was then possible to observe, for the first time, that the ^{3}Car associated with the external antenna of PSI embedded in the thylakoid membranes [69]. The assignment was later confirmed in isolated LHCI complexes [75]. The ^{3}Car associated with PSII have also been investigated by FDMR in thylakoids [76]. However, due to the significant overlap of PSII and PSI

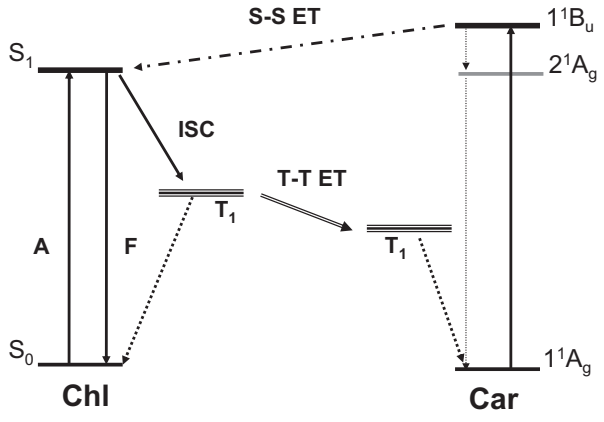

Fig. 1. Scheme describing the principle of FDMR detection of ^{3}Car by monitoring Chl fluorescence emission in photosynthetic systems. On the left it is shown the energy diagram for a Chl molecule, considering its ground (S_0), first singlet excited (S_1) and triplet excited (T_1) states. The Chl T_1 state is populated by intersystem crossing (ISC). On the right, the energy diagram for a Car molecule, considering its ground (1^1A_g), first (2^1A_g) and second (1^1B_u) singlet excited and triplet excited (T_1) states. The Car T_1 state is populated by triplet–triplet energy transfer (TTET) from the Chl triplet. The 1^1B_u singlet excited state of Car is coupled by singlet–singlet energy transfer (SSET) to the S_1 state of Chl. FDMR measurements are possible because the applied microwave field in resonance with a pair of sublevels of the Car T_1 alters the population of the Car ground and singlet excited state. Because of SSET between the Car and Chl molecules, the Chl excited state population is also affected and monitored on its fluorescence emission.

emission above 700 nm, the analysis was limited to a relatively narrow spectral window and led only to a partial characterisation of species belonging to PSII. Nevertheless, it was shown that several ^{3}Car populations are present in PSII: at least one was suggested to be associated to the external antenna and three to the core complex [76].

Here we present an extended and detailed analysis of the ^{3}Car in PSII–LHCII supercomplexes (BBY membranes) and core complexes of PSII isolated from spinach with the aim of identifying the carotenoid molecules involved in the protective quenching of the ^{3}Chl state, in photochemically active particles. The ^{3}Car were characterised employing both the FDMR and the microwave-induced Triplet minus Singlet (T − S) techniques. On the basis of the ZFS parameters and the associated microwave-induced fluorescence spectra (MIF), five ^{3}Car populations were identified in PSII–LHCII and four in the PSII core complex. Thus, four ^{3}Car populations are attributed to β-carotene molecules bound to the core complex. All of them show microwave-induced fluorescence emission maxima which are relatively red-shifted with respect to the bulk emission of both the PSII–LHCII and the isolated core complex.

2. Experimental procedures

2.1. Isolation of PSII–LHCII and PSII core complexes

PSII–LHCII was purified from spinach according to Berthold et al. [77] with the modification described by Dunahay et al. [78] by Triton X-100 fractionation of thylakoids (so-called BBY membranes). Thylakoid membranes were isolated from fresh spinach leaves as described in Ref. [79]. The Chl *a*/*b* ratio determined from water/acetone (20:80) extraction of the purified BBY membranes, using the extinction coefficients given by Lichtenthaler [80], was 2.0 ± 0.1 corresponding to a stoichiometry of approximately 3 LHCII trimers per core complex [3,15,16]. The purity of the preparation was checked by SDS-PAGE, using 15% polyacrylamide gels in 6 M urea (Laemmli discontinuous buffer system [81]) and Western-blot analysis indicating that PSI contamination, as judged by the presence of the high molecular weight subunits PsaA/PsaB, is less than 2%.

The PSII core complex was extracted from the isolated BBY membranes by solubilisation with octyl-β-D-glucopyranoside and successive dialysis, as described by Ghanotakis et al. [82]. After acetone/water extraction Chl *b* was below the level of detection, indicating that the preparation is virtually free of external antenna. The purity of the preparation was confirmed also by SDS-PAGE analysis.

2.2. Optically Detected Magnetic Resonance

FDMR, ADMR and T − S spectra were acquired in a laboratory assembled set-up which has been previously described in detail [46]. In brief, the light from a halogen lamp, powered by a stabilised driver unit, is directed to the sample, immersed in a bath helium cryostat (Oxford Instruments, mod. Spectromag 4), by a system of lenses, filtered through a heat filter and either a 5 cm $CuSO_4$ solution (FDRM) or a water filter (ADMR/T − S), depending on the experiment. The emission is collected by a Si-photodiode (OSI-Centronix) at 45° geometry, through bandpass filters (FWHM ~10 nm) and cut-on filters when necessary to remove the excitation stray light. The absorption is detected with standard geometry though a monochromator (Jobin Yvon, mod. HR250) and the same detector used for fluorescence measurements. The resonator consists of a slow pitch helix. The microwaves source is a HP8559b sweep oscillator equipped with a HP83522s plug-in, amplified by TWT amplifiers (Sco-Nucletudes mod 10-46-30 in the 0.01–1 GHz region, LogMetrics A210/L in the 1–2 GHz region). The microwaves, whose CW power was equivalent to ~1 W, were amplitude-modulated using a laboratory built function generator. The signal from the detector was sent to a Lock-In amplifier (EG&G, mod 5210), whose output was connected to a computer-controlled analogue-to-digital converter. The temperature was 1.8 K in all measurements. Immediately before the insertion into the cryostat, degassed glycerol was added to the samples to a final concentration of 60% v/v, in order to obtain homogeneous and transparent matrices upon freezing. After the dilution, the final Chl concentration of the samples was 150 μg/ml for FDMR experiments and 100 μg/ml for ADMR experiments.

2.3. Data analysis

ODMR is a double resonance technique, which correlates the optical properties of a chromophore with the magnetic resonance transition of its photo-excited triplet state. The resonance frequency depends on the energy separation amongst the triplet sublevel manifolds which, in the absence of an externally applied magnetic field, are determined by the triplet ZFS parameters |D| and |E|. Transitions are observed at energy equivalent to 2|E|, |D| − |E| and |D| + |E|, which in the case of ^{3}Car are all observable. A collection of FDMR records measured at discrete emission wavelengths constitutes, therefore, a data matrix that has one "optical" and one "magnetic" axis. The magnetic axis can be seen as be divided in three sub-sets, each associated with a particular magnetic resonance transition. Because of the correlation between the three magnetic resonance transitions on the "magnetic" axis and the optical properties of the chromophore on the "optical" axis, FDMR data are suitable to be analysed by global fitting procedures.

In the present study the data matrix constituted by the FDMR spectra (acquired in all three 2|E|, |D| − |E| and |D| + |E| transitions and at multiple emission wavelengths) is fitted using a "global constrained" strategy that has been already successfully applied to the investigation of both Chl [66,68] and Car [69,76] triplet states. The global model function is a linear combination of Gaussian functions. The details of the methods are described in Refs. [66,69,70]. A brief account of constrains imposed to the global fit can be summarised as:

i) for each triplet state population, described by a Gaussian sub-band, the peak position describing the 2|E| and the |D| + |E| transitions is common in the simultaneous description of measured spectra at different emission wavelengths. The number of sub-bands and their peak positions are, then, global "free running" fit parameters. The peak position of the |D| − |E| transition is determined from the values of the 2|E| and the |D| + |E| peak transitions; hence they are common to all emission wavelengths but they are not fit parameters [69,76].
ii) ii) for each triplet state population, instead, both the amplitudes and widths of the sub-band sets are "constrained" global fit parameters. The constraint consists in binding the sets of both amplitudes and widths of the sub-bands describing the 2|E| spectrum to those of the associated |D| − |E| and |D| + |E| spectra by scaling constants. Thus, the width and amplitudes of the Gaussian sub-bands describing the 2|E| transition are "free running" global fit and so are the values of the scaling constants.

The imposed constraints are based on the fact that the Gaussian width, dominated by site heterogeneity (inhomogeneous broadening) at 1.8 K, scale proportionally in the different transitions. The constraint on the amplitude is based on the rationale that each sub-band on the "magnetic axis", being associated with a specific chromophore triplet state on the "optical" axis, has an associated microwave induced fluorescence emission (MIF) spectrum whose band shape is expected to be invariant, when observed in the 2|E|, |D| − |E| and |D| + |E| "magnetic" transitions, but for an intensity factor. Moreover, in the measured |D| − |E| transition spectra a sharp negative peak is present that has no counterpart in the other spectral regions. One more sub-band is then necessary to describe the |D| − |E| transition region. This Gaussian sub-band has its frequency position, bandwidth and amplitude as free fit parameters.

The results of the fit analysis are, for each sub-band, the transition energy, from which the ZFS parameters are determined, and the MIF spectrum, which is the plot of the sub-band amplitudes as a function of the detection wavelength.

The number of Gaussian sub-bands required to fit the set of experimental spectra, measured at different emission wavelengths, is estimated as minimal number of fit parameters (i.e. sub-bands) required to yield a good value of the statistical estimators of the fit. To this end, the fitting routine minimises, for n experimental spectra, the "global" estimator χ^2_g by a two-step sequential minimisation employing the Simplex (initial search) and Levenberg–Marquardt (refined search) algorithms. The "local" χ^2_l is estimated, for the i-th spectrum, as the sum of square residual weighted for the shot-noise in the off-resonance tail of the same transition used as an estimator of the variance σ^2, and $\chi^2_g = \frac{N}{N-p}\left(\sum_{l=1}^{n}\chi^2_l\right)\Big/n$, where N is the total number of data points and p is the total number of fit parameters. The quality of the fit is determined by the minimised value of χ^2_g, the inspection of the residual plot and by the stability of the solutions upon their perturbation.

This fit strategy limits the number of free fitting parameters and, then, reduces the number of numerical acceptable solutions, from purely statistic point of view, to a few meaningful physical solutions

3. Results

3.1. Fluorescence Detected Magnetic Resonance of carotenoid triplets in PSII–LHCII

Fig. 2 shows the FDMR spectra detected in the microwave region corresponding to the 2|E|, |D| + |E| and |D| − |E| resonance transitions, monitored at a few representative emission wavelengths across the

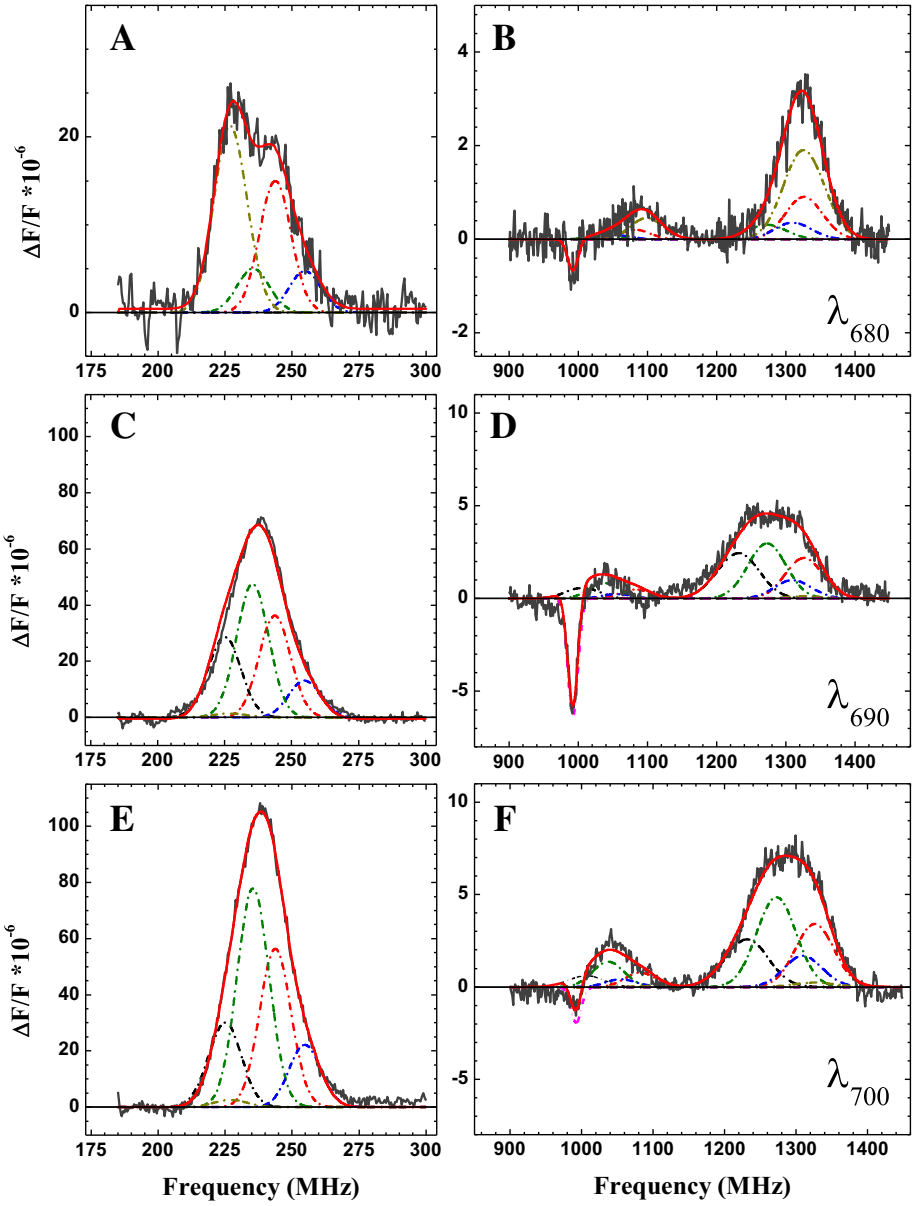

Fig. 2. FDMR spectra of carotenoid triplet states in the PSII–LHCII supercomplex detected at 680 nm (A, B), 690 (C, D) and 700 nm (E, F). Panels A, C and E show the 2|E| transition, whereas panels B, D and F show the |D| + |E| and |D| − |E| transitions. Also shown are the global fits in terms of a linear combination of Gaussian functions. Solid black lines: experimental spectra; red lines: fits. The dash-dotted lines show the contribution of each Gaussian sub-band. Black: T_1^{car} (|D| = 0.0373/|E| = 0.00375 cm^{-1}); red: T_2^{car} (|D| = 0.0402/|E| = 0.00406 cm^{-1}); green: T_3^{car} (|D| = 0.0385/|E| = 0.00393 cm^{-1}); blue: T_4^{car} (|D| = 0.0394/|E| = 0.00425 cm^{-1}); golden: T_5^{car} (|D| = 0.0404/|E| = 0.00378 cm^{-1}); magenta: T^{chl} (992 MHz). Experimental conditions: T = 1.8 K; MW Power: 1 W; mod. Amplitude: 330 Hz; phase: φ = +26°; scan rate: 0.5 MHz sec^{-1}.

fluorescence emission band of the PSII–LHCII complex. The FDMR spectra are equivalent to the corresponding microwave absorption spectra of the triplet states populated under illumination. However, it is not the microwave power which is detected, rather the fluorescence emission since it changes when the steady state populations of the singlet and triplet states are perturbed by the presence of a resonant microwave field (see Supporting information, Appendix 1 for further details on the technique). The FDMR spectra were recorded at a microwave modulation amplitude and phase sensitive detection which is selective for lifetimes in the order of ~10 μs, as expected for ^{3}Car. The intensities of the different transitions ($2|E| \gg |D| + |E| > |D| - |E|$) are characteristic of sublevel populations and anisotropic decay rates of ^{3}Car e.g. [45–48] confirming that the observed FDMR signals arise from these species. Whereas the 2|E| transition (maximum at about 240 MHz) is relatively narrow and well separated from the others, the |D| − |E| (~900–1100 MHz) and |D| + |E| (~1100–1450 MHz) transitions are much broader and partially overlap, indicating the presence of different ^{3}Car populations. At all wavelengths of detection (Figs. 2 and 3), the signals maintain the same polarisation, i.e. positive for the detection settings used in this study. An exception is the presence of a relative sharp negative signal (FWHM ~14 MHz), in the low frequency wing of the |D| − |E| transition, peaking at 992 MHz. This signal has been previously observed in thylakoids from higher plants [66,67] and green algae [68]. It was assigned to a chlorophyll triplet state, probably located in the reaction centre of PSII [67], which is characterised by an unusual fast decay [67,71]. Since the focus of the present study concerns the ^{3}Car in PSII, this fast-decaying ^{3}Chl will be considered in the analysis, because it is necessary to reconstruct the FDMR spectra in region of the carotenoid |D| − |E| transition. Its detailed characterisation will be the subject of further independent investigations.

In order to distinguish the different ^{3}Car populations that contribute to the FDMR signals detected in PSII–LHCII, the data were fitted, globally, by a linear combination of Gaussian functions. As described in the section 2.3 of the Experimental Procedures as well as in previous studies [66,68,76], the global fit poses the constraint that the Gaussian components belonging to the same carotenoid triplet population have also the same microwave-induced fluorescence (MIF) spectrum. Moreover, only the centre position of the Gaussian bands describing the 2|E| and |D| + |E| transitions are free fit parameters, whereas the centre of the |D| − |E| transition is determined from the formers. A minimal number of five Gaussian representing distinct ^{3}Car populations is necessary to describe satisfactorily the FDMR spectra acquired across the whole PSII–LHCII emission. The best global fit parameters are reported in Table 1. Examples of the fit for the 2|E|, |D| + |E| and |D| − |E| transitions are also shown in Fig. 2, whereas the fits across a broader range of emission wavelengths are presented in Fig. 3 for the 2|E| transition. Fig. 4A shows the MIF spectra associated to each of the five carotene populations. The spectrum associated with the abovementioned fast decaying Chl triplet, centred at 992 MHz, is also shown for comparison. Each MIF spectrum derived from the data fitting, is equivalent to the spectrum which would be obtained by scanning the emission wavelengths in the presence of a fixed (amplitude modulated) microwave field, if such ^{3}Car component (in resonance with the microwave field) were the only one present in the complex.

Of the five carotenoid triplet populations resolved by the global fitting analysis, the one described by the ZFS parameters |D| = 0.0404 cm^{-1}, |E| = 0.00378 cm^{-1} (T_5^{car}) has a particularly blue-shifted MIF (Fig. 4A), characterised by a maximum at ~680 nm and relatively weak intensity at detection wavelengths above 690 nm. It should be noted that, the contribution of T_5^{car} to the sub-band decomposition across most of the emission band is almost negligible (Figs. 2 and 3). Nevertheless, its presence is necessary when a global fit analysis of the entire set of measured spectra is considered, due to a significant presence of this contribution in the FDMR spectra monitored in the

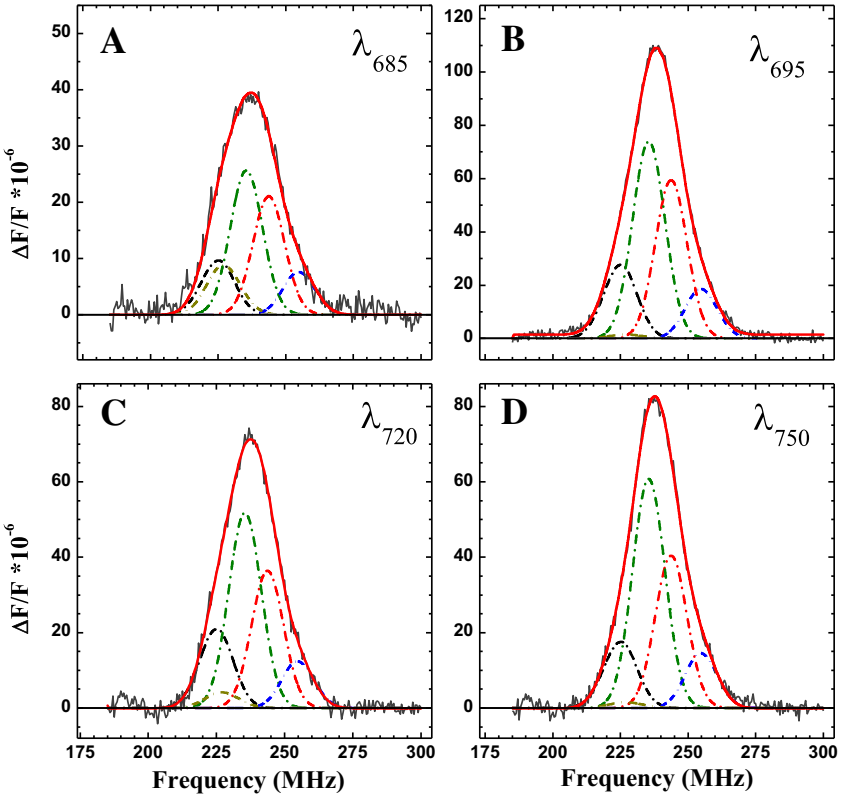

Fig. 3. 2|E| FDMR transition of carotenoid triplet states in the PSII–LHCII supercomplex, detected at 685 (A), 695 (B), 720 (C) and 750 nm (D). The black lines are the experimental spectra, the reds lines are the results of the global fit in terms of linear combinations of Gaussian functions. The dash-dotted lines show the contribution of each Gaussian sub-band. Black: T_1^{car} (|D| = 0.0373/|E| = 0.00375 cm^{-1}); red: T_2^{car} (|D| = 0.0402/|E| = 0.00406 cm^{-1}); green: T_3^{car} (|D| = 0.0385/|E| = 0.00393 cm^{-1}); blue: T_4^{car} (|D| = 0.0394/|E| = 0.00425 cm^{-1}); golden: T_5^{car} (|D| = 0.0404/|E| = 0.00378 cm^{-1}). Experimental conditions as in the legend of Fig. 2.

Table 1
Global fit of the FDMR spectra recorded in the PSII–LHCII supercomplex.

	2|E|		|D| − |E|		|D| + |E|		ZFS	
	Centre (MHz)	FWHM (MHz)	Centre (MHz)	FWHM (MHz)	Centre (MHz)	FWHM (MHz)	|D| (cm^{-1})	|E| (cm^{-1})
T_1^{car}	225 ± 3	14.4 ± 0.5	1233 ± 18	71 ± 9	1008 ± 18	57 ± 7	0.0373	0.00375
T_2^{car}	244 ± 6	13.8 ± 0.5	1326 ± 23	63 ± 7	1082 ± 24	51 ± 6	0.0402	0.00406
T_3^{car}	235 ± 6	14.0 ± 0.3	1272 ± 23	65 ± 8	1037 ± 24	52 ± 7	0.0385	0.00393
T_4^{car}	255 ± 6	13.9 ± 0.4	1309 ± 25	63 ± 7	1055 ± 26	50 ± 6	0.0394	0.00425
T_5^{car}	227 ± 5	14.5 ± 0.5	1325 ± 15	69 ± 10	1098 ± 16	55 ± 7	0.0404	0.00378

Fit parameters retrieved from the global analysis of the FDMR spectra in the 680–760 nm interval, decomposed in terms of a linear combination of Gaussian sub-bands.

680–685 nm emission window (Figs. 2–4). Whereas the 2|E| transition associated to the T_5^{car} population is substantially overlapped with that of another population (T_1^{car}, Fig. 2 and Table 1), the |D| + |E| and |D| − |E| transitions are more distinguished.

This is also apparent in the MIF spectrum retrieved from the fit (Fig. 4A). By comparison with low temperature fluorescence emission spectra of the isolated LHCII complex, that peaks in the 682–684 nm interval [83–89], it is possible to assign the ^{3}Car population associated with the most blue-shifted MIF, to a triplet state populated in PSII external antenna.

On the other hand, the MIF spectra of the remaining ^{3}Car populations have maximal intensity in the 690–710 nm window. In particular the two populations characterised by |D| = 0.0373 cm^{-1}, |E| = 0.00375 cm^{-1} (T_1^{car}) and |D| = 0.0385 cm^{-1}, |E| = 0.00393 cm^{-1} (T_3^{car}) have the most red-shifted maxima, peaking at about 705 nm. These MIF spectra also show a pronounced shoulder at 695 nm, which is more evident for the case of T_1^{car}, whereas for T_3^{car} it is more intense resulting in a relatively flat maximum between 695 and 705 nm (Fig. 4A). The MIF spectra associated with the populations characterised by the larger ZFS parameters |D| = 0.0402 cm^{-1}, |E| = 0.00406 cm^{-1} (T_2^{car}) and |D| = 0.0394 cm^{-1}, |E| = 0.00425 (T_4^{car}) have maxima at 695 and 700 nm, respectively. In the case of T_2^{car} the MIF also displays a shoulder in the 685–690 nm range and some residual intensity at shorter emission wavelengths, which is much weaker for the T_4^{car} population. An interesting feature that characterises all of the ^{3}Car MIF spectra (excluding the T_5^{car} population) is that they also display large intensities at wavelengths longer than 710 nm. This is a remarkable red-shift with respect to the maximum of the emission spectrum of the PSII enriched membranes [89–91], peaking at 695 nm also in our experimental conditions (data not shown). This feature is further highlighted by the comparison with the MIF spectrum of the fast-decaying Chl population that has a well defined maximum at about 690 nm, and significantly less intensity in the fluorescence emission tail.

The spectral window above 690 nm could be satisfactorily fitted considering only four Gaussian components, without significant differences either of the ZFS or of the associated MIF spectra (data not presented). This indicates that a fifth Gaussian component is only necessary when considering the short-wavelength emission in the 680–685 nm interval, providing further confirmation that the T_5^{car} is specifically coupled to blue-shifted Chl emission forms. Moreover, the red-shift of all the other ^{3}Car -associated MIF spectra is independent on the exact number of fitting components.

An increase in the relative intensity of the MIF spectra in the long wavelength emission tail is expected as they are measured as ΔF/F ratios (see Discussion). Nevertheless, in Fig. 4A the MIF spectra associated with the different ^{3}Car populations are compared with the MIF spectrum belonging to a ^{3}Chl likely associated with the reaction centre, which does not show remarkable intensity above 710 nm instead. Since this ^{3}Chl was detected in the same sample and experimental conditions as the ^{3}Car, it can be used as an internal reference, indicating that at least two ^{3}Car populations are indeed coupled by energy transfer to low-energy Chl *a* spectral forms, and that the increased intensity in the long-wavelength emission tail of the MIF spectra is not solely due to spectral distortion deriving from the representation in terms of ΔF/F ratios.

The lowest Chl *a* transition energies in PSII have often been suggested to be associated with chromophores bound to the proximal antenna complexes CP43 and CP47 e.g. [49,53,92–95]. Moreover, it has also been suggested that red-shifted transitions are present in the reaction centre complex [96–99]. To further investigate this issue we have conducted a parallel investigation in the isolated core complex of PSII.

3.2. Fluorescence Detected Magnetic Resonance of carotenoid triplets in the PSII core

Fig. 5 shows the FDMR spectra recorded in the isolated core complex of PSII, at characteristic emission wavelengths, under the same

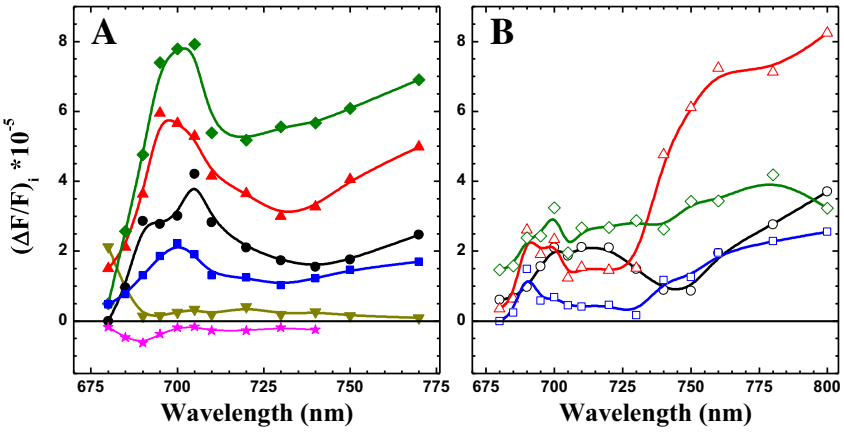

Fig. 4. Microwave-induced fluorescence emission spectra (MIF) derived from the global analysis of the FDMR spectra recorded in the PSII–LHCII supercomplex (A, solid symbols) and the PSII core complex (B, open symbols). Black lines and circles: $T_{1,(c)}^{car}$; red lines and triangles: $T_{2(c)}^{car}$; green lines and diamonds: $T_{3(c)}^{car}$; blue lines and squares: $T_{4(c)}^{car}$; golden lines and downward-triangles: T_5^{car} (PSII–LHCII only). In panel A the MIF of the fast-decaying ^{3}Chl (magenta and stars) detected at 992 MHz, is also shown for comparison; note the opposite sign of the signal. Intensities are scaled on the 2|E| transition.

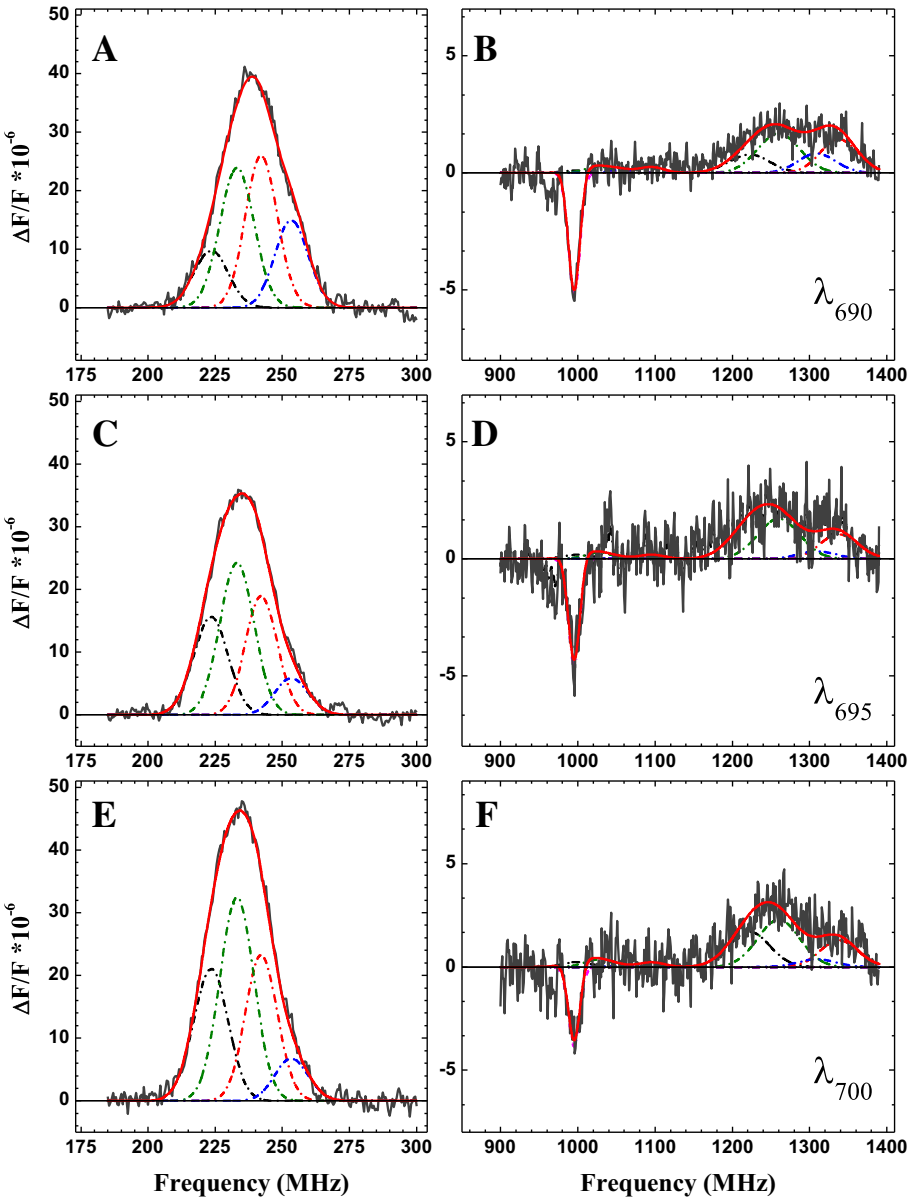

Fig. 5. FDMR spectra of carotenoid triplet states in the isolated PSII core complex detected at 690 (A, B), 695 (C, D) and 700 nm (E, F). Panels A, C and E show the 2|E| transition, whereas panels B, D and F show the |D| + |E| and |D| − |E| transitions. The black lines are the experimental spectra, the red lines are the results of the global fit in terms of linear combinations of Gaussian functions. The dash-dotted lines show the contribution of each Gaussian sub-band. Black: $T_{1,c}^{car}$ (|D| = 0.0370/|E| = 0.00373 cm^{-1}); red: $T_{2,c}^{car}$ (|D| = 0.0406/|E| = 0.00404 cm^{-1}); green: $T_{3,c}^{car}$ (|D| = 0.0381/|E| = 0.00389 cm^{-1}); blue: $T_{4,c}^{car}$ (|D| = 0.0394/|E| = 0.00422 cm^{-1}); magenta: T^{chl} (995 MHz). Experimental conditions as in the legend of Fig. 2.

experimental conditions employed for the PSII–LHCII supercomplex. The FDMR spectra recorded in the PSII core share some characteristics with those presented in Fig. 2, in terms of polarisation, peak positions and relative intensities of the 2|E|, |D| + |E| and |D| − |E| transitions. The presence of a sharp negative feature peaking at ~995 MHz is also observed, further supporting the previous assignment of this signal to a ^{3}Chl state associated to the PSII core complex [66,67,71]. In order to investigate the contribution of different ^{3}Car populations, the FDMR spectra have been globally decomposed by a linear combination of Gaussian functions. Four populations are sufficient to describe the data across the whole emission spectrum. The global fit parameters resulting from the fits are reported in Table 2. Representative fits for the 2|E|, |D| + |E|

Table 2
Global fit of the FDMR spectra recorded in the PSII core complex.

	2|E|		|D| − |E|		|D| + |E|		ZFS	
	Centre (MHz)	FWHM (MHz)	Centre (MHz)	FWHM (MHz)	Centre (MHz)	FWHM (MHz)	|D| (cm^{-1})	|E| (cm^{-1})
$T_{1,c}^{car}$	224 ± 5	15.2 ± 0.6	1222 ± 30	62 ± 8	998 ± 31	41 ± 5	0.0370	0.00373
$T_{2,c}^{car}$	242 ± 6	14.0 ± 0.5	1337 ± 34	57 ± 6	1095 ± 34	38 ± 4	0.0406	0.00404
$T_{3,c}^{car}$	233 ± 5	15.0 ± 0.5	1260 ± 36	64 ± 8	1027 ± 36	42 ± 5	0.0381	0.00389
$T_{4,c}^{car}$	253 ± 6	14.6 ± 0.5	1309 ± 36	57 ± 7	1056 ± 36	38 ± 5	0.0394	0.00422

Fit parameters retrieved from the global analysis of the FDMR spectra in the 680–800 nm interval, decomposed in terms of a linear combination of Gaussian sub-bands.

and |D| − |E| transitions are also presented in Fig. 5, and over a wider fluorescence emission wavelength interval (2|E| only) in Fig. 6.

The ^{3}Car population observed in the BBY membranes, characterised by |D| = 0.0404 cm^{-1}, |E| = 0.00378 cm^{-1} and blue-shifted MIF spectrum (Table 1, Fig. 4A), is absent in the core complex, confirming its assignment to a carotenoid triplet state populated in the external antenna.

The peak positions and hence the ZFS parameters associated to the four ^{3}Car detected in the PSII core complex do not differ significantly from those observed in PSII–LHCII (compare Tables 1 and 2). However, the MIF spectra appear more structured (Fig. 4B) in the bulk emission wavelength between 685 and 710 nm, and show substantial intensity at wavelength longer than 730 nm. Although this was also observed in the PSII–LHCII complex (Fig. 4A), the intensity of the tail above 710 nm is further increased in PSII core.

The MIF spectra associated with the populations having ZFS |D| = 0.0370 cm^{-1}, |E| = 0.00373 cm^{-1} ($T^{car}_{1,c}$) and |D| = 0.0381 cm^{-1}, |E| = 0.00389 cm^{-1} ($T^{car}_{3,c}$) have the most red-shifted maxima in the bulk emission, peaking at 700 nm (Fig. 4B). Based on the ZFS comparison, they can be correlated to the PSII–LHCII ^{3}Car populations that displayed the most red-shifted MIF spectra, although the maximum is ~5 nm blue-shifted in the PSII core complex. The broad shoulders observed at 690 nm for $T^{car}_{1,c}$ and at 685 nm for $T^{car}_{3,c}$ are also 5–10 nm blue-shifted with respect to what observed in the PSII–LHCII. On the other hand, the intensity of the MIF spectra at detection wavelength longer than 710 nm increases for both ^{3}Car populations.

The MIF spectra associated with the populations characterised by |D| = 0.0406 cm^{-1}, |E| = 0.00404 cm^{-1} ($T^{car}_{2,c}$) and |D| = 0.0394 cm^{-1}, |E| = 0.00422 ($T^{car}_{4,c}$), that have the largest values for the ZFS parameters, show maxima at 690 nm. In the case of $T^{car}_{2,c}$ the MIF also displays a secondary peak at 700 nm, which appears just as a weak shoulder for the $T^{car}_{4,c}$ population. In both cases, significant intensity is observed in the red emission tail above 730 nm; this is particularly remarkable for $T^{car}_{2,c}$.

Taken together, these results suggest that the four populations observed in the core complex correspond to those observed in the

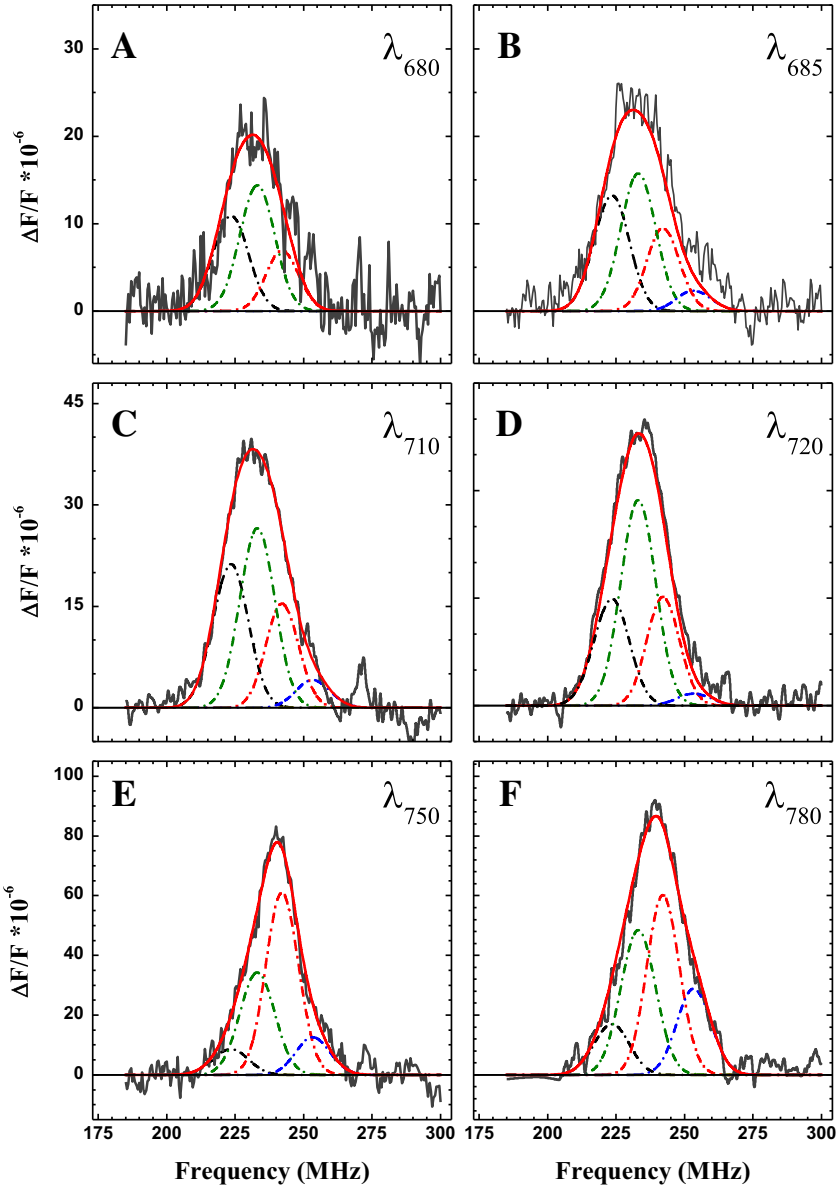

Fig. 6. 2|E| FDMR transition of carotenoid triplet states in the isolated PSII core complex detected at 680 (A), 685 (B), 710 (C), 720 (D), 750 (E) and 780 nm (F). The black lines are the experimental spectra, the red lines are the results of the global fit in terms of linear combinations of Gaussian functions. The dash-dotted lines show the contribution of each Gaussian sub-band. Black: $T^{car}_{1,c}$ (|D| = 0.0370/|E| = 0.00373 cm^{-1}); red: $T^{car}_{2,c}$ (|D| = 0.0406/|E| = 0.00404 cm^{-1}); green: $T^{car}_{3,c}$ (|D| = 0.0381/|E| = 0.00389 cm^{-1}); blue: $T^{car}_{4,c}$ (|D| = 0.0394/|E| = 0.00422 cm^{-1}). Experimental conditions as in the legend of Fig. 2.

PSII–LHCII membranes, with the exclusion of the one that can be assigned to a ^{3}Car belonging to the external antenna. Therefore the ^{3}Car populations observed in the core of PSII are assigned to triplet states sitting on β-Car molecules ($^3\beta$ - Car), since this is the only carotenoid present in the complex. The slight variation in the ZFS and the blue-shift of the MIF spectra (~5 nm on average within the spectra resolution of the technique) observed in the core complex point towards subtle re-arrangements of both the β-Car molecules and the emitting Chls, upon removal of the external antenna. This could be either an effect of the binding of the antenna complexes to the core, leading to fine structural rearrangements of the pigments, or an effect of the biochemical procedure employed in the purification of the core complex.

3.3. Triplet minus Singlet spectra of carotenoids in the core and PSII–LHCII complexes

In order to gain further insight into the nature of the ^{3}Car detected in PSII, these were further investigated, both in the core and in the PSII–LHCII complex, by microwave-induced Triplet minus Singlet (T − S) spectroscopy. These spectra are detected by scanning the transmission wavelength in the presence of an amplitude modulated microwave field at a given frequency, which in this case was set at values close to the maxima observed in the 2|E| transition by FDMR. In Fig. 7 the T − S spectra recorded in PSII–LHCII, upon microwave pumping in the 2|E| transition at 230 MHz, 237 MHz and 245 MHz are presented. The T − S spectra recorded in the PSII core complex upon microwave excitation at 224 MHz, 235 MHz and 245 MHz are shown in Fig. 8. In both samples a clear dependence of the T − S profile on the microwave excitation frequency is observed. This is the result of selective excitation of different triplet populations at the different microwave pump frequencies. In order to resolve the different $T_1 \rightarrow T_n$ transitions (and associated ground state bleaching), the T − S spectra recorded in the PSII core and PSII–LHCII complexes were fitted to a linear combination of Gaussian functions. The results of the fit analysis are reported in Table 3. The $T_1 \rightarrow T_n$ absorption is dominated, both in the PSII–LHCII and in the PSII core complexes by three species with maxima at 518, 527 and 538 nm. A weak component with a red-shifted maximum at 553 nm is obtained by the fit of the data only in PSII–LHCII. The most red-shifted $T_1 \rightarrow T_n$ absorption is observed preferentially by excitation at 230 MHz and with lower relative intensity by excitation at 237 MHz. This component seems to be associated to the T_5^{car} population detected in PSII–LHCII that has a maximum in the 2|E| at 227 MHz and is attributed to a ^{3}Xan populated in the external antenna. Previous studies performed on isolated LHCII showed the presence of $T_1 \rightarrow T_n$ transitions peaking at 505 and 525 nm [45,48,50,55,57]. The $T_1 \rightarrow T_n$ transition centred at 505 nm was not observed in our measurements, presumably because it is being masked by the singlet bleaching of the red-most carotenes ($^3\beta$ − Car). In view of these uncertainties and due to its very weak signal intensity it is not possible, at present, to give further information concerning the T_5^{car} triplet population.

\All the other transitions, also based on the FDMR results, are attributed to $^3\beta$ - Car in the core. Although they are observed upon excitation at all the microwave frequencies employed in this study, their relative contribution to the T − S spectra depends on the specific excitation. The shortest $T_1 \rightarrow T_n$ transition, peaking at 518 nm, is observed preferentially in the isolated PSII core and in PSII–LHCII upon 245 MHz excitation, hence upon preferential excitation of the triplet population with the larger |E| ZFS parameter. These correspond to the $T_{2(c)}^{car}$(that peaks at ~243 MHz in the 2|E| transition) and to a lesser extent to the $T_{4(c)}^{car}$ component, peaking at ~254 MHz (Tables 1 and 2). Interestingly the $T_{2(c)}^{car}$ and $T_{4(c)}^{car}$populations are also associated with the less red-shifted MIF spectra, peaking at 695/700 and 690 nm in PSII–LHCII and PSII core respectively. On the other hand, the more intense relative contribution of the most red-shifted $^3\beta$ - Car transition (538 nm) is observed upon excitation at 225–230 MHz, which selects preferentially the $T_{1(c)}^{car}$populations in the PSII–LHCII and the PSII core complexes. This is the ^{3}Car that shows the most red-shifted MIF. On the other hand, the maximal relative contribution of the $T_1 \rightarrow T_n$ transition peaking at 527 nm, is detected for excitation close to the maximum of the 2|E| transition (235–237 MHz). These pump frequencies excite preferentially the most intense ^{3}Car ($T_{3(c)}^{car}$) that displays a rather red-shifted MIF, peaking between 700 and 705 nm.

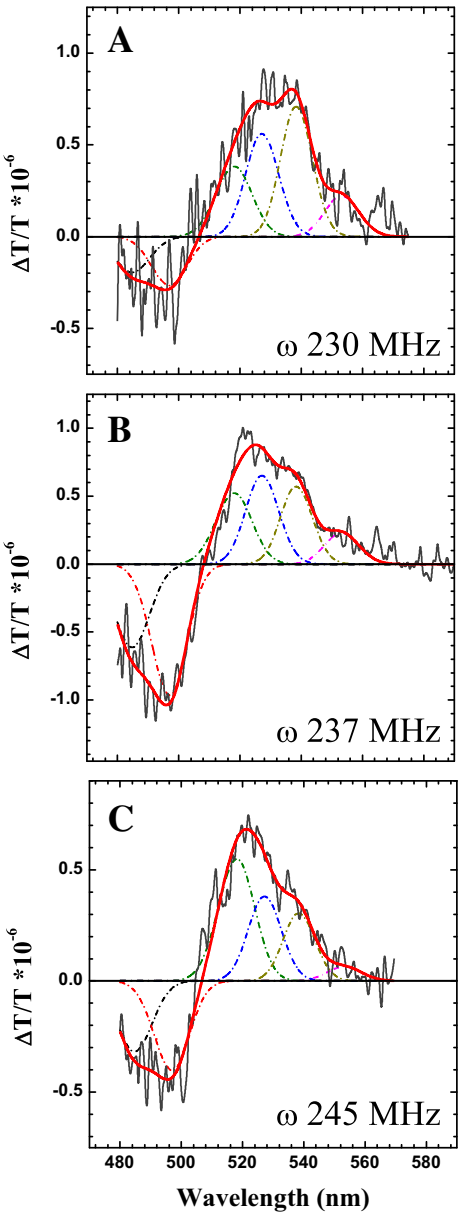

Fig. 7. Microwave-induced T − S spectra of carotenoid triplet states in the PSII–LHCII supercomplex upon selective excitation in the 2|E| transition: 230 MHz (A), 237 MHz (B) and 245 MHz (C). Black solid lines: experimental data; red solid lines: fits; dash-dotted lines: Gaussian sub-bands. Fit parameters are reported in Table 3. Experimental conditions: T = 1.8 K; MW Power: 1 W; mod. Amplitude: 330 Hz; phase: φ = −154°; time constant: 3 s; slit width: 1.0 nm.

4. Discussion

Quenching of the ^{3}Chl by carotenoids represents a fundamental photoprotective strategy in photosynthetic systems, as it prevents the sensitisation of $^1O_2$. Although the crucial physiological importance of this process is generally acknowledged (reviewed in Refs. [3,11–19,22]), and several studies have been performed to gain insights into the nature of the ^{3}Car populated in isolated Chl/Car-binding complexes [45–57], the characterisation of these species in relatively intact systems,

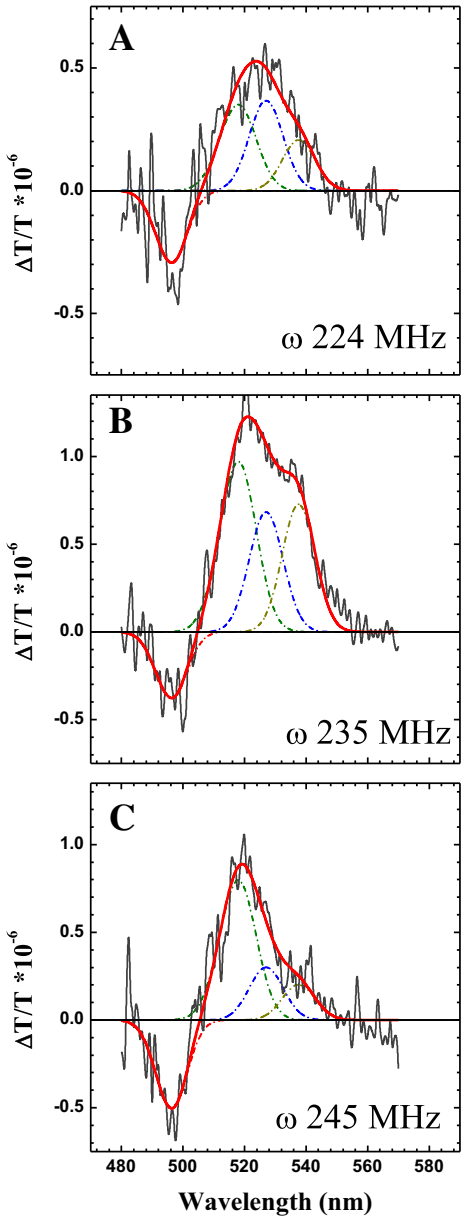

Fig. 8. Microwave-induced T − S spectra of carotenoid triplet states in the PSII core complex upon selective excitation in the 2|E| transition: 224 MHz (A), 235 MHz (B) and 245 MHz (C). Black solid lines: experimental data; red solid lines: fits; dash-dotted lines: Gaussian sub-bands. Fit parameters are reported in Table 3. Experimental conditions as in the legend of Fig. 7.

Table 3
Global fits of the T − S spectra in PSII–LHCII and PSII core.

PSII–LHCII				PSII core		
	Centre (nm)	FWHM (nm)	Assignment	Centre (nm)	FWHM (nm)	Assignment
Band 1	484 ± 2	13 ± 2	$S_0 \rightarrow S_1$	486 ± 3	13 ± 3	$S_0 \rightarrow S_1$
Band 2	497 ± 2	14 ± 2	$S_0 \rightarrow S_1$	496 ± 2	12 ± 3	$S_0 \rightarrow S_1$
Band 3	518 ± 1	14 ± 2	$T_1 \rightarrow T_n$	517 ± 4	14 ± 4	$T_1 \rightarrow T_n$
Band 4	527 ± 1	13 ± 2	$T_1 \rightarrow T_n$	527 ± 2	13 ± 3	$T_1 \rightarrow T_n$
Band 5	538 ± 1	12 ± 2	$T_1 \rightarrow T_n$	538 ± 3	13 ± 3	$T_1 \rightarrow T_n$
Band 6	553 ± 4	13 ± 3	$T_1 \rightarrow T_n$	–	–	–

Fit parameters retrieved from the global analysis of the T − S spectra in the PSII–LHCII and the PSII core complex, decomposed in terms of a linear combination of Gaussian sub-bands.

such as whole photosystems, remains rather incomplete due to spectral crowding. Because of the crucial photoprotective action of ^{3}Chl quenching by Cars through the TTET mechanism, the identification of ^{3}Car and ^{3}Chl in more intact, photochemically active, complexes represents a significant step in the understanding of the physiological role of these chromophores.

Therefore, in this study we have performed a comparative analysis of ^{3}Car in the PSII–LHCII supercomplex and the PSII core complex by ODMR, a technique that allows correlating the magnetic resonance frequencies between the triplet sublevel manifold with the optical properties of the chromophores carrying the triplet state. It was then possible to identify five ^{3}Car populations in the isolated PSII–LHCII and their associated MIF spectra and ZFS parameters. The latter are in substantial agreement with those retrieved from the FDMR analysis of isolated thylakoid membranes [76]. However, the analysis of PSII ^{3}Car in thylakoids was limited to the 680–695 nm fluorescence emission range because at longer wavelengths the PSI emission precludes their selective detection. The present improved analysis of ^{3}Car in the isolated PSII–LHCII and PSII core complexes allows the assignment of four of the detected populations to β-Car triplet states located in the core complex and one ^{3}Car populated in the external antenna of PSII. Since ODMR measurements are performed at cryogenic temperatures (1.8 K), the singlet excited state distribution is different from that encountered at room temperature, as it tends to be localised on the lowest energy Chl forms. It is therefore possible that more ^{3}Car than those observed in our current analysis are populated at physiological temperatures. Nonetheless, the ^{3}Car observed here, particularly those attributed to β-Car molecules of the core complex, are expected to be observed also at room temperature since, although less markedly, the low energy forms present in this complex are expected to carry (relatively) more excited state population than the "bulk" of the emission. On the other hand, at low temperature most of the excited states are localised in the core complex because of the presence of red-shifted transitions [83,84,88–90] with respect to outer antenna [85–87]. Therefore, the Car involved in triplet quenching in the external antenna bound to the core of PSII might largely escape detection in our measurements. In this respect, it is also interesting to note that the stoichiometry of Car binding is larger for the external antenna than the core complexes e.g. [3,10–13]. This issue will likely require further investigations by complementary techniques which allow measurements to be performed at, or near, room temperature.

In the following paragraphs we will discuss, separately, the characterisation of the ^{3}Xan and ^{3}Car associated with the external antenna and the core complex of PSII detected in this study.

4.1. Carotenoid triplet states in PSII external antenna

One ^{3}Car population ($|D| = 0.0404\ cm^{-1}$, $|E| = 0.00378\ cm^{-1}$) is observed in PSII–LHCII but not in the core complex, and it is therefore attributed to a ^{3}Xan populated in the external antenna. This assignment is consistent with the observation of a blue-shifted MIF spectrum associated to this triplet, displaying maximal intensity at 680 nm. In fact, it has been previously shown that at low temperatures the maximal emission of the isolated LHCII complex peaks at 683–685 nm e.g. [85–87], i.e. 5–10 nm to the blue with respect to those of CP43 and CP47 [51–54], the PSII core complex [49,88,90] and the whole photosystem [83,84,89]. It is however interesting to note that the previous FDMR analysis of thylakoid membranes [76] suggested the presence of two ^{3}Xan. The ZFS parameters of the population detected in PSII–LHCII closely agree with those of the most intense component attributed to ^{3}Xan in thylakoids [76]. The second ^{3}Xan detected in the membranes had a relative intensity of about one third of the dominating one. Since the intensity of the FDMR at the shortest emission wavelengths is weaker in the isolated PSII–LHCII compared to thylakoids, it is possible that the less intense ^{3}Xan either falls below the level of detection, or that it is not discerned by the fit analysis. Moreover, it has often been reported that part of

the LHCII antenna, on average one trimer per core complex, is lost during the isolation of PSII–LHCII e.g. [3,15,16]. Thus the weakening of the FDMR signals at 680–685 nm with respect to those detected at 690–695 nm could also be related to the decrease of the external antenna size during the purification of PSII.

The values of the ZFS parameters of the T_5^{car} population are in fairly good agreement with those determined in the isolated LHCII complex, even though, as for the analysis of thylakoids, at least two ^{3}Xan have been detected in the isolated complex by the ODMR techniques [45–47,55]. Still, some differences are observed, as previously noticed [76] in the analysis of the isolated thylakoids, that might be the result of either a perturbation of the carotenoids bound to LHCII upon biochemical isolation or subtle changes in the binding of the chromophores occurring when the antenna is bound to the photosystem, i.e. closer to its natural environment. Further investigations are required to gain more conclusive evidence on this matter.

4.2. Carotenoid triplet states in the core of PSII

The remaining four triplet populations are attributed to $^3\beta$ - Car species as they are characterised by the same set of ZFS parameters, within the confidence limits of the FDMR Gaussian decomposition analysis, in both PSII–LHCII and PSII core complexes. The improvement in the quality of MIF spectra (Fig. 4) obtained in the present study, compared to the previous analysis of thylakoids, shows that all the $^3\beta$ - Car are associated with relatively low-energy Chl forms present in the core, with emission maxima between 695 and 705 nm. The MIF spectra of the $^3\beta$ - Car characterised by |D| = 0.0370/0.0373 cm^{-1}, |E| = 0.00373/0.00375 cm^{-1} ($T_{1(c)}^{car}$) and |D| = 0.0381/0.0385 cm^{-1}, |E| = 0.00389/0.00393 cm^{-1} ($T_{3(c)}^{car}$), have maxima at about 705 nm in the PSII–LHCII supercomplex and 700 nm in the core. In both cases, shoulders in the 690–695 nm interval are also observed, although with different intensities.

The MIF spectra of the other two $^3\beta$ - Car populations characterised by |D| = 0.0406/0.0402 cm^{-1}, |E| = 0.00404/0.00406 cm^{-1} ($T_{2(c)}^{car}$) and |D| = 0.0394 cm^{-1}, |E| = 0.00422/0.00425 cm^{-1} ($T_{4(c)}^{car}$) are instead coupled to less red-shifted Chl forms having maximal emission at about 690–695 nm, being generally 5 nm red-shifted in PSII–LHCII with respect to the core complex. The MIF spectra also show shoulders at about 700–705 nm. Another interesting observation, that is common to all the $^3\beta$ - Car resolved in the analysis, is that the MIF spectra show pronounced intensity at wavelength longer than 710 nm, that is clearly outside the main fluorescence emission band.

The interpretation of MIF spectra requires some considerations. First, at the low temperature at which the measurements are performed (<2 K), the fluorescence emission from the system is expected to stem exclusively from the lowest energy transition within the pigment array, acting as a terminal emitter. Yet it is commonly reported, particularly for large particles such as whole photosystems or core complexes, that the emission derives from more than one spectral form e.g. [83,84,88–90]. These observations can be explained considering the presence of barriers for excited state equilibration in the energetic landscape of pigment system comprising about 40 Chls, in the case of the core complex, and 200–250 Chls, in the case of PSII–LHCII. These energy barriers tend to localise the excited states in more than one "local" energy minimum, representing local energy sinks. These forms can be either proper low-temperature terminal emitters, i.e. being completely energetically uncoupled from the others, or pre-equilibrated emitters, in the case that the energy transfer rates amongst the local emitters are comparable to the excited state lifetimes of the low energy chromophores.

Second, it should be noted that the MIF spectra are presented as $\Delta F/F$ ratios. For a single chromophore the $\Delta F/F$ ratio should assume the same value across the emission band, including the long wavelength tail that arise from vibrational modes strongly coupled to the $S_0 \rightarrow S_1$ transition. This explains, qualitatively, the long wavelength tail observed in the spectra of all the $^3\beta$ - Car populations. On the other hand, structured MIF spectra imply the overlapping emission of more than one chromophore, thereby rendering their interpretation less straightforward. Hence, we have performed simulations considering a simplified kinetic and spectral scheme which yields realistic (but not quantitative) information. The details of the MIF spectra simulations are presented in Appendix 2 of Supporting information. In the following we only discuss the principal outcomes derived from the calculations. Based on the qualitative simulations it is argued that in order to obtain MIF spectra having band shapes compatible to the experimental results, it is necessary that the $^3\beta$ - Car are populated by TTET energy transfer from ^{3}Chl representing local emitters, coupled by slow singlet–singlet ($S - S$) energy transfer to red Chls, acting as terminal emitters (see Fig. S5 of Supporting information). On the contrary, the direct population of $^3\beta$ - Car by a long wavelength Chl form, as well as the rapid energy transfer between the sensitising (local) Chl and the low energy (terminal) emitter results in calculated MIF spectra which are not in agreement with the experimental ones. Therefore, the analysis suggests that although the maximal MIF intensity is observed around 700–705 nm, resulting from the emission of relatively red-shifted Chl forms present in the core of PSII, the $^3\beta$ - Car is initially sensitised by Chl forms that are blue-shifted by 10–15 nm with respect to the lower energy states in the complex.

4.3. Comparison of MIF spectra attributed to β-carotene triplets with low energy states of the isolated core complexes

This study reveals the presence of Chl forms in the core of PSII having maximal emission at about 705 nm. In order to address their possible location within the complex, it is interesting to discuss previous literature reports concerning the lowest energy transitions in the core, and in the isolated core antenna complexes, CP43 and CP47. Whereas there is a general agreement concerning the lowest transition energies in the isolated core antenna complexes, their assignment to specific chromophores is still debated [51,91–94]. The lowest energy state in the isolated CP47 complex is identified as a Chl *a* form having maximal absorption at 690 nm and emission at 695 nm [51,91–94]. At least one other Chl *a* form having maximal absorption at 684–685 nm and emission at 686–688 nm is present in this complex [51,91–94,100]. In CP43 two degenerate states both characterised by maximal absorption around 683 nm, but having significant different bandwidths (one being almost tree time as broad as the other), have been identified [54,94–96]. The maximal emission of CP43 at low temperature peaks between 684 and 686 nm, even though an intense shoulder at ~690 nm is also observed [54,94–96,100]. However, in none of the isolated core antenna complexes, to our knowledge, Chl forms with emission maxima close to 700–710 nm, have been resolved.

On the other hand, the energy of the lowest energy state in the reaction centre (which is isolated as the D1D2Cytb_{559} complex) is more controversial. This is because there is a host of experimental evidences, particularly from the analysis of the T − S spectra associated with the recombination triplet state and hole-burning spectroscopy, that the site energies are perturbed upon biochemical isolation of the D1D2Cytb_{559} complex [74,96–98,101]. Thus, the most reliable information are retrieved from the study of the core complex which also harbours CP43 and CP47. In the core complex, as well as in the BBY particles, the bleaching associated with the population of the recombination triplet peaks in the 684–686 nm interval [74,96–98], and a further shift to 687 nm was observed in isolated thylakoids [66,67]. For an average Stokes' shift of 3–4 nm, as commonly observed for Chl *a* in photosynthetic complexes, the Chl carrying the recombination triplet, which at low temperatures is likely to be the so-called Chl_{D1} molecule, is expected to emit between 687 and 690 nm, i.e. almost iso-energetic to the CP43 lower energy states. However, Chl_{D1} appears to be, based on the structural models [8,9], too distant from the two β - Car molecules coordinated by the RC to allow triplet–triplet energy transfer. Intriguingly, the presence of a weak and broad emission

form, having a maximal absorption between 700 and 705 nm and a suggested emission extending above 780 nm, has also been reported [97–99]. The rate of singlet–singlet ($S-S$) energy transfer of this spectral form with the other chromophores in the system must, however, be particularly weak, otherwise it would represent by far the lowest energy state in PSII, from which all the emission, at low temperatures, is expected to stem from, as observed from the so-called red-forms of PSI e.g. [3,11,102,103]. Moreover, the emission of such "deep-red form" species is excessively red-shifted to be correlated to the 705 nm emission form observed in the FDMR measurements. Thus, the 700–705 nm emission form resolved in this study appears to be distinct from the deep-red form which has been previously reported [97–99]. As just discussed, this newly resolved emission form does not appear to correlate with any of the lowest emitters observed either in the isolated RC or in core antenna complexes, CP43/CP47. Since it is observed in the whole core complex (but also in the PSII–LHCII supercomplex), it is likely that this state is either strongly perturbed by the isolation procedure required to obtain the proximal antenna complexes, or that it represents a state generated by exciton coupling between chromophores at the interface of the proximal antenna and the RC complex.

4.4. Assignment of β-carotene triplets to specific sites of PSII core complex

The emission peaks detected in the core of PSII and in the BBY membranes at 685 and 695 nm at cryogenic temperatures have been suggested to be correlated with the emission of the low energy states of CP43 and CP47, respectively [88–90], acting as terminal emitters uncoupled in terms of energy transfer. The MIF spectra associated with $^3\beta$ - Car are all red-shifted with respect to the maximum of the emission spectrum of both complexes (due, as stated above, to the weak $S-S$ energy coupling with a red-shifted Chl emitting at about 705 nm). Still, in the 685–700 nm interval, the MIF spectra show features that overlap with the proximal antenna low energy states. Although the lowest energy forms present in the RC also fall in a similar range, those have been attributed to photochemically active pigments, which are essentially uncoupled to carotenoids. In fact, the MIF of the fast decaying Chl triplet (FDMR peaking at 992–995 MHz) has maximal (absolute) intensity at 690 nm and very weak intensity in all of the red-emission tail [66,67] and is therefore markedly blue-shifted with respect to those attributed to $^3\beta$ - Car (Fig. 4A).

On the basis of the previous discussion, we tentatively assign the most red-shifted $T^{car}_{1(c)}$ and $T^{car}_{3(c)}$ populations to $^3\beta$ - Car populated in the CP47 complex since it harbours the lowest energy Chl states of PSII proximal antenna. The observation of intense features at ~700 nm in the MIF of both these triplet populations is interpreted as a preferential singlet energy coupling of CP47 triplet sensitising Chl forms with the state emitting at 705 nm. The remaining populations ($T^{car}_{2(c)}$ and $T^{car}_{4(c)}$) are then assigned to states populated either in CP43 or in the peripheral pigments of the RC complex. These sensitising Chl forms appear more weakly coupled by $S-S$ energy transfer to the 705 nm emitting Chl form.

4.5. Tuning of the fine spectroscopic properties of β-carotene in the PSII core complex

Finally, it is interesting to note that the difference between the highest and the lowest $T_1 \rightarrow T_n$ β - Car transition, observed in the T − S spectra (Figs. 7 and 8, Table 3), is about 20 nm. Hence, the binding of the same chromophore (β - Car) to specific protein sites leads to rather remarkable tuning of its electronic transition energies. Such an effect is comparable to that expected for a progressive increase of the conjugation length of the chromophore e.g. [104–106]. Recently this protein fine-tuning of the electronic properties of carotenoids, in addition to their well known dependence from the polarisability of the surrounding [107], has been demonstrated to depend also on the alteration of the effective conjugation length, through steric hindrance acting on the conjugated end cycles [108]. This observation is in full agreement with the results presented here. Actually, amongst the triplet states assigned to core β-Car, the components $T^{car}_{2(c)}$ and $T^{car}_{4(c)}$, which have large |D| values, have a correspondent blue-shifted absorption (518 nm), as both properties depend on the number of conjugated double bonds [109]. On the contrary, the component $T^{car}_{1(c)}$, characterised by the smallest |D| value amongst the various components, concomitantly has the most red-shifted transition (528 nm). Hence, the modulation of the optical properties of the β-Cars in the different sites depends, at least in part, on their effective conjugation length. It is also worth noticing that the β-Car populations displaying the most blue-shifted $T_1 \rightarrow T_n$ transition also have the most blue-shifted MIF spectrum, and vice versa for the most red-shifted ones. This can be rationalized in terms of the fine tuning of the protein-mediated acceptor-donor pair properties, in order to optimise the efficiency of both singlet and triplet energy transfer.

5. Conclusions

The parallel investigation of Car triplet states in the PSII–LHCII supercomplex and the PSII core complex by ODMR techniques allowed us to resolve four $^3\beta$-Car populations in the core complex and one ^{3}Xan population in the external antenna.

Two of the detected ^{3}Car, $T^{car}_{1(c)}$ and $T^{car}_{3(c)}$, are populated by Chl forms coupled by weak singlet–singlet interactions to a low energy state having maximal emission at about 705 nm. These populations show a maximal $T_1 \rightarrow T_n$ transition between 527 and 538 nm, representing the most red-shifted absorption amongst PSII $^3\beta$ - Car. We tentatively localise these $^3\beta$ - Car components in the CP47 core antenna. The remaining populations ($T^{car}_{2(c)}$ and $T^{car}_{4(c)}$), which show a weaker $S-S$ energy coupling to the 705 nm emitter, are tentatively assigned to $^3\beta$-Car triplets populated in the CP43 complex.

Moreover, the results highlight the presence of Chl spectral forms in the core complex of PSII absorbing/emitting at longer wavelengths (10–15 nm red-shifted) than the photochemical reaction centre.

These triplets states, observed at low temperature when the excitation is localised on a few pre-equilibrated emitters, are expected to be populated also at physiological temperatures when the excitation is more delocalised over the entire array of antenna chromophores. Even though it is likely that other ^{3}Car will be populated at higher temperatures, particularly in the external antenna whose singlet excited state is depopulated at low temperature, the populations detected in the present study are still expected to be present and therefore play an important role in photo-protection. We consider that their identification represents a first, yet necessary, step to get a more in depth understanding of their physiological role.

Acknowledgements

This research was in part founded by the grant PRIN2010/2011 Prot. 2010FM738P awarded to D.C. from the Italian Ministry of Education, Universities and Research (MIUR). We thank Prof. Robert Jennings (University of Milan) for fruitful discussion.

Appendix A. Supplementary data

Appendix 1 described the basic principle of the ODMR technique. Appendix 2 describes in detail the kinetic and spectral model utilised for the simulations of the microwave-induced fluorescence emission spectra. Supplementary data to this article can be found online at http://dx.doi.org/10.1016/j.bbabio.2014.11.008.

References

[1] B.A. Diner, F. Rappaport, Structure, dynamics, and energetics of the primary photochemistry of photosystem II of oxygenic photosynthesis, Annu. Rev. Plant Biol. 53 (2002) 551–580.

[2] N. Nelson, C.F. Yocum, Structure and function of photosystems I and II, Annu. Rev. Plant Biol. 57 (2006) 521–565.
[3] S. Caffarri, T. Tibiletti, R.C. Jennings, S. Santabarbara, A comparison between plant Photosystem I and Photosystem II architecture and functioning, Curr. Protein Pept. Sci. 15 (2014) 296–331.
[4] T. Cardona, A. Sedoud, N. Cox, A.W. Rutherford, Charge separation in photosystem II: a comparative and evolutionary overview, Biochim. Biophys. Acta Bioenerg. 1817 (2012) 26–43.
[5] J.P. Allen, J.C. Williams, The evolutionary pathway from anoxygenic to oxygenic photosynthesis examined by comparison of the properties of photosystem II and bacterial reaction centers, Photosynth. Res. 107 (2011) 59–69.
[6] A.G. Koziol, T. Borza, K. Ishida, P. Keeling, R.W. Lee, D.G. Durnford, Tracing the evolution of the light-harvesting antennae in chlorophyll a/b-containing organisms, Plant Physiol. 143 (2007) 1802–1816.
[7] M. Ballottari, J. Girardon, L. Dall'osto, R. Bassi, Evolution and functional properties of photosystem II light harvesting complexes in eukaryotes, Biochim. Biophys. Acta Bioenerg. 1817 (2012) 143–157.
[8] A. Zouni, H.T. Witt, J. Kern, P. Fromme, N. Krauss, W. Saenger, P. Orth, Crystal structure of photosystem II from *Synechococcus elongatus* at 3.8 Å resolution, Nature 409 (2001) 739–743.
[9] Y. Umena, K. Kawamaki, N. Kamiya, Crystal structure of oxygen-evolving photoystem II at a resolution of 1.9 Å, Nature 473 (2011) 55–60.
[10] R. Bassi, B. Pineau, P. Dainese, J. Marquardt, Carotenoid-binding proteins of photosystem II, Eur. J. Biochem. 212 (1993) 297–303.
[11] R. Jennings, G. Zucchelli, R. Bassi, Antenna structure and energy transfer in higher plant photosystems, in: J. Mattay (Ed.), Topics in Current Chemistry, vol. 177, Spinger-Verlag, Berlin, Heidelberg, Germany, 1996, pp. 147–181.
[12] D. Sandonà, R. Croce, A. Pagano, M. Crimi, R. Bassi, Higher plants light harvesting proteins. Structure and function as revealed by mutation analysis of either protein or chromophore moieties, Biochim. Biophys. Acta Bioenerg. 1365 (1998) 207–214.
[13] H. van Amerongen, R. Croce, Light harvesting in photosystem II, Photosynth. Res. 116 (2013) 251–263.
[14] X. Pan, Z. Liu, M. Li, W. Chang, Architecture and function of plant light-harvesting complexes II, Curr. Opin. Struct. Biol. 23 (2013) 515–525.
[15] R. Kouřil, J.P. Dekker, E.J. Boekema, Supramolecular organization of photosystem II in green plants, Biochim. Biophys. Acta Bioenerg. 1817 (2012) 2–12.
[16] S. Caffarri, R. Kouřil, S. Kereïche, E.J. Boekema, R. Croce, Functional architecture of higher plant photosystem II supercomplexes, EMBO J. 28 (2009) 3052–3063.
[17] P. Horton, A.V. Ruban, R.G. Walters, Regulation of light harvesting in green plants, Annu. Rev. Plant Physiol. Plant Mol. Biol. 47 (1996) 655–684.
[18] A.V. Ruban, M.P. Johnson, Xanthophylls as modulators of membrane protein function, Arch. Biochem. Biophys. 504 (2010) 78–85.
[19] D. Siefermann-Harms, Carotenoids in photosynthesis. I. Location in photosynthetic membranes and light-harvesting function, Biochim. Biophys. Acta 811 (1985) 325–355.
[20] H.A. Frank, R. Cogdell, Photochemistry and function of carotenoids in photosynthesis, in: A. Young, G. Britton (Eds.), Carotenoids in Photosynthesis, Chapman and Hall, London, United Kingdom, 1993, pp. 253–326.
[21] A. Rivadossi, G. Zucchelli, F.M. Garlaschi, R.C. Jennings, Light absorption by the chlorophyll a/b complexes of photosystem II in a leaf with special reference to LHCII, Photochem. Photobiol. 80 (2004) 492–498.
[22] B. Demmig-Adams, Carotenoids and photoprotection in plants: a role for the xanthophyll zeaxanthin, Biochim. Biophys. Acta Bioenerg. 1020 (1990) 1–24.
[23] B. Robert, P. Horton, A.A. Pascal, A.V. Ruban, Insights into the molecular dynamics of plant light-harvesting proteins *in vivo*, Trends Plant Sci. 9 (2004) 385–390.
[24] A.A. Pascal, Z.F. Liu, K. Broess, B. van Oort, H. van Amerongen, C. Wang, P. Horton, B. Robert, W.R. Chang, A. Ruban, Molecular basis of photoprotection and control of photosynthetic light-harvesting, Nature 436 (2005) 134–137.
[25] A.V. Ruban, R. Berera, C. Ilioaia, I.H.M. van Stokkum, J.T.M. Kennis, A.A. Pascal, H. van Amerongen, B. Robert, P. Horton, R. van Grondelle, Identification of a mechanism of photoprotective energy dissipation in higher plants, Nature 450 (2007) 575–578.
[26] N.E. Holt, D. Zigmantas, L. Valkunas, X.P. Li, K.K. Niyogi, G.R. Fleming, Carotenoid cation formation and the regulation of photosynthetic light harvesting, Science 307 (2005) 433–436.
[27] T.K. Ahn, T.J. Avenson, M. Ballottari, Y.C. Cheng, K.K. Niyogi, R. Bassi, G.R. Fleming, Architecture of a charge-transfer state regulating light harvesting in a plant antenna protein, Science 320 (2008) 794–797.
[28] M. Zubik, R. Luchowski, W. Grudzinski, M. Gospodarek, I. Gryczynski, Z. Gryczynski, J.W. Dobrucki, W.I. Gruszecki, Light-induced isomerization of the LHCII-bound xanthophyll neoxanthin: possible implications for photoprotection in plants, Biochim. Biophys. Acta Bioenerg. 1807 (2013) 1237–1243.
[29] F.G. Plumley, G.W. Schmidt, Reconstitution of Chl a/b light-harvesting complexes. Xanthophyll-dependent reconstitution and energy transfer, Proc. Natl. Acad. Sci. U. S. A. 84 (1987) 145–150.
[30] E. Formaggio, G. Cinque, R. Bassi, Functional architecture of the major light-harvesting complex from higher plants, J. Mol. Biol. 314 (2001) 1157–1166.
[31] K. Humbeck, S. Romer, H. Senger, Evidence for an essential role of carotenoids in the assembly of an active photosystem II, Planta 179 (1989) 242–250.
[32] J.A. Bautista, F. Rappaport, M. Guergova-Kuras, R.O. Cohen, J.H. Golbeck, J.Y. Wang, D. Béal, B.A. Diner, Biochemical and biophysical characterization of photosystem I from phytoene desaturase and zeta-carotene desaturase deletion mutants of *Synechocystis* sp. PCC 6803: evidence for PsaA- and PsaB-side electron transport in cyanobacteria, J. Biol. Chem. 280 (2005) 20030–20041.
[33] S. Santabarbara, A.P. Casazza, K. Ali, C.K. Economou, T. Wannathong, F. Zito, K.E. Redding, F. Rappaport, S. Purton, The requirement for carotenoids in the assembly and function of the photosynthetic complexes in *Chlamydomonas reinhardtii*, Plant Physiol. 161 (2013) 535–546.
[34] T.G. Truscott, The photophysics and photochemistry of the carotenoids, J. Photochem. Photobiol. B 6 (1990) 359–371.
[35] H.A. Frank, R.J. Cogdell, Carotenoids in photosynthesis, Photochem. Photobiol. 63 (1996) 257–264.
[36] P.G. Bowers, G. Porter, Quantum yield of triplet formation in solutions of chlorophylls, Proc. R. Soc. A 296 (1967) 435–441.
[37] A.A. Krasnovsky, Delayed luminescence and phosphorescence of plant pigments, Photochem. Photobiol. 36 (1992) 733–741.
[38] H. Kramer, P. Mathis, Quantum yield and rate of formation of the carotenoid triplet state in photosynthetic structure, Biochim. Biophys. Acta Bioenerg. 593 (1980) 319–329.
[39] P. Mathis, W.L. Butler, K. Satoh, Carotenoid triplet state and chlorophyll fluorescence quenching in chloroplasts and subchloroplast particles, Photochem. Photobiol. 30 (1979) 603–614.
[40] C. Wolff, H.T. Witt, On metastable states of carotenoids in primary events of photosynthesis, Z. Naturforsch. 24b (1969) 1031–1037.
[41] A.A. Krasnovsky, Photoluminescence of singlet oxygen in pigment solutions, Photochem. Photobiol. 29 (1979) 29–36.
[42] A. Krieger-Liszkay, Singlet oxygen production in photosynthesis, J. Exp. Bot. 56 (2005) 337–346.
[43] T. Javorfi, G. Garab, K.R. Naqvi, Reinvestigation of the triplet-minus-singlet spectrum of chloroplasts, Spectrochim. Acta A 56 (2000) 211–214.
[44] A. Sonneveld, H. Rademaker, L.N.M. Duysens, Transfer and trapping of excitation energy ion photosystem II as studied by chlorophyll fluorescence quenching by dinitrobenzene and carotenoid triplet. The matrix model, Biochim. Biophys. Acta Bioenerg. 593 (1980) 272–289.
[45] R. Van der Vos, D. Carbonera, A.J. Hoff, Microwave and optical spectroscopy of carotenoid triplets in light-harvesting complex LHCII of spinach by absorbance-detected magnetic resonance, Appl. Magn. Reson. 2 (1991) 179–202.
[46] D. Carbonera, G. Giacometti, G. Agostini, FDMR of carotenoid and chlorophyll triplets in light-harvesting complex LHCII of spinach, Appl. Magn. Reson. 3 (1992) 361–368.
[47] D. Carbonera, G. Giacometti, G. Agostini, A. Angerhofer, V. Aust, ODMR of carotenoid and chlorophyll triplets in CP43 and CP47 complexes of spinach, Chem. Phys. Lett. 194 (1992) 275–281.
[48] R. Van der Vos, E.M. Franken, A.J. Hoff, ADMR study of the effect of oligomerisation on the carotenoid triplet and triplet–triplet energy transfer in light harvesting complex II (LHC II) of spinach, Biochim. Biophys. Acta Bioenerg. 1188 (1994) 243–250.
[49] M.-L. Groot, E.J. Peterman, I.H.M. van Stokkum, J.P. Dekker, R. van Grondelle, Temperature dependent triplet and fluorescence quantum yield of photosystem II described in a thermodynamic model, Biophys. J. 67 (1994) 318–330.
[50] E.J.G. Peterman, F.M. Dekker, R. van Grondelle, H. Van Amerongen, Chlorophyll a and carotenoid states in light harvesting complex II of higher plants, Biophys. J. 59 (1995) 2670–3678.
[51] M.-L. Groot, E.J. Peterman, I.H. van Stokkum, J.P. Dekker, R. van Grondelle, Triplet and fluorescing states of the CP47 antenna complex of photosystem II studied as a function of temperature, Biophys. J. 68 (1995) 281–290.
[52] V. Barzda, E.J.G. Peterman, R. van Grondelle, H. van Amerongen, The influence on triplet formation in light-harvesting chlorophyll a/b pigment–protein complex II of green plants, Biochemistry 37 (1998) 546–551.
[53] R. Schödel, K.-D. Irrgang, J. Voigt, G. Renger, Rate of carotenoid triplet formation in solubilised light-harvesting complex II (LHCII) from spinach, Biophys. J. 75 (1998) 3143–3153.
[54] M.-L. Groot, R.N. Frese, F. deWeerd, K. Bromek, Å. Petterson, E.J.G. Peterman, I.H.M. van Stokkum, R. van Grondelle, J.P. Dekker, Spectroscopic properties of the CP43 core antenna protein of photosystem II, Biophys. J. 77 (1999) 3328–3340.
[55] S.S. Lampoura, V. Barzda, G.M. Owen, A.J. Hoff, H. van Amerongen, Aggregation of LHCII leads to a redistribution of the triplets over the central xanthophylls in LHCII, Biochemistry 41 (2002) 9139–9144.
[56] R. Croce, M. Mozzo, T. Morosinotto, A. Romeo, R. Hienerwadel, R. Bassi, Singlet and triplet state transitions of carotenoids in the antenna complexes of higher-plant photosystem I, Biochemistry 46 (2007) 3846–3855.
[57] M. Mozzo, L. Dall'Osto, R. Hienerwadel, R. Bassi, R. Croce, Photoprotection in the antenna complexes of photosystem II: role of individual xanthophylls in chlorophyll triplet quenching, J. Biol. Chem. 283 (2008) 6184–6192.
[58] K. Akiyama, S. Terokubota, T. Ikoma, Y. Ikegami, Spin Polarization conservation during intramolecular triplet–triplet energy transfer studied by Time-Resolved EPR Spectroscopy, J. Am. Chem. Soc. 116 (1994) 5324–5327.
[59] R. Bittl, E. Schlodder, I. Geisenheimer, W. Lubitz, R.J. Cogdell, Transient EPR and absorption studies of carotenoid triplet formation in purple bacterial antenna complexes, J. Phys. Chem. B 105 (2001) 5525–5553.
[60] M. Di Valentin, F. Biasibetti, S. Ceola, D. Carbonera, Identification of the sites of chlorophyll triplet quenching in relation to the structure of LHC-II from higher plants. Evidence from EPR spectroscopy, J. Phys. Chem. B 113 (2009) 13071–13078.
[61] D. Carbonera, A. Agostini, M. Di Valentin, C. Gerotto, S. Basso, G.M. Giacometti, T. Morosinotto, Photoprotective sites in the violaxanthin–chlorophyll a binding Protein (VCP) from *Nannochloropsis gaditana*, Biochim. Biophys. Acta Bioenerg. 1837 (2014) 1235–1246.
[62] M. Di Valentin, E. Meneghin, A. Polimeno, C. Büchel, E. Salvadori, C.W.M. Kay, D. Carbonera, Triplet–triplet energy transfer in fucoxanthin-chlorophyll protein from diatom *Cyclotella meneghiniana*: insights into the structure of the complex, Biochim. Biophys. Acta Bioenerg. 1827 (2013) 1226–1234.

[63] R.H. Clarke, Triplet state ODMR spectroscopy, in: R.H. Clarke (Ed.), Techniques and Applications to Biophysical Systems, Wiley-Interscience, New York, U.S.A. 1982
[64] A.J. Hoff, Optically detected magnetic resonance of triplet states, in: A.J. Hoff (Ed.), Advanced EPR, Elsevier, Amsterdam, The Netherlands1989.
[65] D. Carbonera, Optically Detected Magnetic Resonance (ODMR) of photoexcited triplet states, Photosynth. Res. 102 (2009) 403–414.
[66] S. Santabarbara, E. Bordignon, R.C. Jennings, D. Carbonera, Chlorophyll triplet states associated with photosystem II of thylakoids, Biochemistry 41 (2002) 8184–8194.
[67] S. Santabarbara, R.C. Jennings, D. Carbonera, Analysis of photosystem II triplet states in thylakoids by fluorescence detected magnetic resonance as a function of the reduction state of the primary quinone acceptor Q_A, Chem. Phys. 294 (2003) 257–267.
[68] S. Santabarbara, G. Agostini, A.P. Casazza, C.D. Syme, P. Heathcote, F. Böhles, M.C.W. Evans, R.C. Jennings, D. Carbonera, Chlorophyll triplet states associated with Photosystem I and Photosystem II in thylakoids of the green alga *Chlamydomonas reinhardtii*, Biochim. Biophys. Acta Bioenerg. 1767 (2007) 88–105.
[69] S. Santabarbara, D. Carbonera, The carotenoid triplet state associated with the long wavelength emitting chlorophyll forms of Photosystem I in isolated thylakoid membranes, J. Phys. Chem. B 109 (2005) 986–991.
[70] S. Santabarbara, K.V. Neverov, F.M. Garlaschi, G. Zucchelli, R.C. Jennings, Involvement of uncoupled antenna chlorophylls in photoinhibition in thylakoids, FEBS Lett. 491 (2001) 109–113.
[71] W.O. Feikema, P. Gast, I.B. Klenina, I.I. Proskuryakov, EPR characterisation of the triplet state in photosystem II reaction centers with singly reduced primary acceptor Q_A, Biochim. Biophys. Acta Bioenerg. 1709 (2005) 105–112.
[72] H.J. Den Blanken, A.J. Hoff, A.P.J.M. Jongenelis, B.A. Diner, High-resolution triplet-minus singlet absorbance difference spectroscopy of photosystem II particles, FEBS Lett. 157 (1983) 21–27.
[73] F. VanMiegem, W. Nitschke, P. Mathis, A.W. Rutherford, The influence of the quinone–iron electron acceptor complex on the reaction centre photochemistry of Photosystem II, Biochim. Biophys. Acta 977 (1989) 207–214.
[74] D. Carbonera, G. Giacometti, G. Agostini, A well resolved ODMR triplet minus singlet spectrum of P680 from PSII particles, FEBS Lett. 343 (1994) 200–204.
[75] D. Carbonera, G. Agostini, T. Morosinotto, R. Bassi, Quenching of chlorophyll triplet states by carotenoids in reconstituted Lhca4 subunit of peripheral light-harvesting complex of photosystem I, Biochemistry 44 (2005) 8337–8346.
[76] S. Santabarbara, G. Agostini, P. Heathcote, D. Carbonera, A fluorescence detected magnetic resonance investigation of the carotenoid triplet states associated with photosystem II of isolated spinach thylakoid membranes, Photosynth. Res. 86 (2005) 283–296.
[77] D.A. Berthold, G.T. Babcock, C.F. Yocum, A highly resolved, oxygen-evolving photosystem II preparation from spinach thylakoid membranes, FEBS Lett. 134 (1981) 231–234.
[78] T.G. Dunahay, L.A. Stahelin, M. Seibert, P.G. Ogilvie, S.P. Berg, Structural, biochemical, and biophysical characterisation of four oxygen-evolving photosystem II preparation from spinach, Biochim. Biophys. Acta Bioenerg. 764 (1984) 179–193.
[79] R.C. Jennings, F.M. Garlaschi, P.D. Gerola, R. Etzion-Katz, G. Forti, Proton-induced grana formation in chloroplast. Distribution of chlorophyll–protein complexes and photosytem II photochemistry, Biochim. Biophys. Acta Bioenerg. 638 (1981) 100–107.
[80] H.K. Lichtenthaler, Chlorophyll and carotenoids: pigments of photosynthetic membranes, Methods Enzymol. 148 (1987) 350–382.
[81] U.K. Laemmli, Cleavage of structural proteins during the assembly of the head of bacteriophage T4, Nature 227 (1970) 680–685.
[82] D.F. Ghanotakis, D.M. Demetriou, C.M. Yocum, Isolation and characterization of an oxygen-evolving photosystem II reaction center core preparation and a 28 kDa chl-binding protein, Biochim. Biophys. Acta Bioenerg. 891 (1987) 15–21.
[83] R. Strasser, W.L. Butler, Fluorescence emission spectra of photosystem I, photosystem II and the light-harvesting chlorophyll a/b complex of higher plants, Biochim. Biophys. Acta Bioenerg. 462 (1977) 307–313.
[84] C.P. Rijgersberg, J. Amesz, A.P. Thielen, J.A. Swager, Fluorescence emission spectra of chloroplasts and subchloroplast preparations at low temperature, Biochim. Biophys. Acta Bioenerg. 637 (1981) 272–277.
[85] E.J.G. Peterman, S.F. Hobe, F. Calkoen, R. van Grondelle, H. Paulsen, H. van Amerongen, Low temperature spectroscopy of monomeric and trimeric form of reconstituted light-harvesting chlorophyll a/b complex, Biochim. Biophys. Acta Bioenerg. 1273 (1996) 171–174.
[86] A.V. Ruban, J.P. Dekker, P. Horton, R. van Grondelle, Temperature dependence of chlorophyll fluorescence from the light harvesting complex II of higher plants, Photochem. Photobiol. 61 (1995) 216–221.
[87] G. Zucchelli, F.M. Garlaschi, R.C. Jennings, Thermal broadening analysis of the light harvesting complex II absorption spectrum, Biochemistry 35 (1996) 16247–16254.
[88] E. Krausz, J.L. Hughes, P.J. Smith, R.J. Pace, S.P. Arsköld, Assignment of the low-temperature fluorescence in oxygen-evolving photosystem II, Photosynth. Res. 84 (2005) 193–199.
[89] E.G. Andrizhiyevskaya, A. Chojnicka, J.A. Bautista, B.A. Diner, R. van Grondelle, J.P. Dekker, Origin of the F685 and F695 fluorescence in photosystem II, Photosynth. Res. 84 (2005) 173–180.
[90] M. Mimuro, S. Akimoto, T. Tomo, M. Yokono, H. Miyashita, T. Tsuchiya, Delayed fluorescence observed in the nanosecond time region at 77 K originates directly from the photosystem II reaction center, Biochim. Biophys. Acta Bioenerg. 1767 (2007) 327–334.
[91] M. Reppert, K. Acharya, B. Neupane, R. Jankowiak, Lowest electronic states of the CP47 antenna protein complex of photosystem II: simulation of optical spectra and revised structural assignments, J. Phys. Chem. B 114 (2010) 11884–11898.
[92] B. Neupane, N.C. Dang, K. Acharya, M. Reppert, V. Zazubovich, R. Picorel, M. Seibert, R. Jankowiak, Insight into the electronic structure of the CP47 antenna protein complex of photosystem II: hole burning and fluorescence study, J. Am. Chem. Soc. 132 (2010) 4214–4219.
[93] M. Reppert, V. Zazubovich, N.C. Dang, M. Seibert, R. Jankowiak, Low-energy chlorophyll states in the CP43 antenna protein complex: simulation of various optical spectra. II, J. Phys. Chem. B 112 (2008) 9934–9947.
[94] A.P. Casazza, M. Szczepaniak, M.G. Müller, G. Zucchelli, A.R. Holzwarth, Energy transfer processes in the isolated core antenna complexes CP43 and CP47 of photosystem II, Biochim. Biophys. Acta Bioenerg. 1797 (2010) 1606–1616.
[95] N.C. Dang, V. Zazubovich, M. Reppert, B. Neupane, R. Picorel, M. Seibert, R. Jankowiak, The CP43 proximal antenna complex of higher plant photosystem II revisited: modelling and hole burning study, J. Phys. Chem. B 112 (2008) 9921–9933.
[96] P.J. Smith, S. Peterson, V.M. Masters, T. Wydrzynski, S. Styring, E. Krausz, R.J. Pace, Magneto-optical measurements of the pigments in fully active photosystem II core complexes from plants, Biochemistry 41 (2002) 1981–1989.
[97] S.P. Arsköld, V.M. Masters, B.J. Prince, P.J. Smith, R.J. Pace, E. Krausz, Optical spectra of synechocystis and spinach photosystem II preparations at 1.7 K: identification of the D1-pheophytin energies and stark shifts, J. Am. Chem. Soc. 125 (2003) 13063–13074.
[98] E. Krausz, N. Cox, S.P. Arsköld, Spectral characteristics of PS II reaction centres: as isolated preparations and when integral to PS II core complexes, Photosynth. Res. 98 (2008) 207–217.
[99] J. Morton, J. Hall, P. Smith, F. Akita, F.H. Koua, J.R. Shen, E. Krausz, Determination of the PS I content of PS II core preparations using selective emission: a new emission of PS II at 780 nm, Biochim. Biophys. Acta Bioenerg. 1837 (2014) 167–177.
[100] G. Raszewski, T. Renger, Light harvesting in photosystem II core complexes is limited by the transfer to the trap: can the core complex turn into a photoprotective mode? J. Am. Chem. Soc. 130 (2008) 4431–4446.
[101] K. Acharya, V. Zazubovich, M. Reppert, R. Jankowiak, Primary electron donor(s) in isolated reaction center of photosystem II from *Chlamydomonas reinhardtii*, J. Phys. Chem. B 116 (2012) 4860–4870.
[102] R. Croce, G. Zucchelli, F.M. Garlaschi, R.C. Jennings, A thermal broadening study of the antenna chlorophylls in PSI-200, LHCI, and PSI core, Biochemistry 37 (1998) 17355–17360.
[103] R. Croce, H. van Amerongen, Light-harvesting in photosystem I, Photosynth. Res. 116 (2013) 153–166.
[104] H. Hashimoto, Y. Koyama, K. Ichimura, T. Kobayashi, Time resolved absorption spectroscopy of triplet states produced from the all-tran, 7-cis, 9-cis, 13-cis, 15-cis isomers of β-carotene, Chem. Phys. Lett. 162 (1989) 517–522.
[105] P. Mathis, J. Kleo, The triplet state of β-carotene and analog polyene of different length, Photochem. Photobiol. 18 (1973) 343–346.
[106] Y. Koyama, H. Hashimoto, Spectroscopy of carotenoids in carotenoids in photosynthesis, in: A. Young, G. Britton (Eds.), Chapman & Hall, London, UK1983.
[107] K. Hirayama, Absorption spectra and chemical structure. II. Solvent effect, J. Am. Chem. Soc. 77 (1955) 379–381.
[108] M.M. Mendes-Pinto, D. Galzerano, A. Telfer, A.A. Pascal, B. Robert, C. Ilioaia, Mechanisms underlying carotenoid absorption in oxygenic photosynthetic proteins, J. Biol. Chem. 288 (2013) 18758–19765.
[109] G. Araki, T. Murai, Molecular structure and absorption spectra of carotenoids, Progr. Theor. Phys. 8 (1952) 639–654.